

Lead Free Perovskite Materials: Interplay of Metals Substitution for Environmentally Compatible Solar Cells Fabrication

Ahmed Esmail Shalan^a, Samrana Kazim^a and Shahzada Ahmad^{a,b*}

^a BCMaterials-Basque Center for Materials, Applications and Nanostructures, Martina Casiano, UPV/EHU Science Park, Barrio Sarriena s/n, Leioa 48940, Spain

Tel: +34 946128811 Email: shahzada.ahmad@bcmaterials.net

^b IKERBASQUE, Basque Foundation for Science, Bilbao, 48013, Spain

Abstract:

Perovskite solar cells have attracted significant attention during the current decade due to their efficacy and photovoltaics performance, which has reached to a new millstone in thin film category. Albeit perovskite solar cells have witnessed a remarkable 24.2% light to electricity conversion efficiency, but the ubiquity of lead metal due to its dual toxicity behaviour towards human as well as environment, apart from material instability are the current bottlenecks towards its possible commercial endeavour. This allowed the scientific community to explore other metal ions as substitution for lead metal, while preserving the unique properties of lead to produce environment-friendly perovskite structure. In this review, we put forward the highlights on the recent developments and challenges of lead-free hybrid halide perovskite based light harvester for solar cell application. This will allow the research community to discover materials library for ideal sustainable technology.

Corresponding Authors: E-mail: (S. A.): shahzada.ahmad@bcmaterials.net

1. Introduction

The effect of climate change is fuelling and deleterious effect is being witnessed, immediate actions are required along with strong political and technological revolution for transition to clean energy. In most part of the world, carbon neutral energy is competitive over fossil fuels and to accelerate this transition, we need a paradigm shift in our approach. Among renewable sources, photovoltaics (PV) and wind have shown grid parity and >100GW of solar was installed alone in 2018. Currently, utility-based PV capacity are dominated by silicon-based technology. Due to the societal commitments and needs, thin film based PV are expected to disrupt the market. During the last two decades, sincere efforts have been laid in the research direction on thin film based PV, CdTe, CIGS or CZTS were initially referred as thin film PV along with amorphous silicon, due to their commercialization. Emerging PV were termed as nanostructured photovoltaics, and research are being made on organic photovoltaics (OPV), dye sensitized solar cells (DSSCs), quantum dot solar cells (QDSC) and perovskite solar cells (PSCs). Researchers and technologist has made earnest efforts during the current decade, which allowed to push the solar-to-electricity power conversion efficiency (PCE) of PSCs from mere 3.8% to 24.2%. The obtained PCE supersede with that of other mature thin-film based PV involving copper indium gallium selenide (CIGS), with 22.9%, and CdTe, with 22.1%.^[1a] The PSCs employs low materials usage, diversity in using an array of deposition process, possibility to use a variety of charge transport materials (n and p type) with respect to active perovskite layer. The device architect is very versatile in terms of design and composition and avoid dependency on single raw materials. In the state-of-the-art, the high performance is mainly represented by lead halide based perovskites, but a trade-off exists between high performance and stability together with the toxicity induced by the presence of lead (Pb). Currently Pb is the indispensable material in high performance PSCs and its usage is being debated politically as well as technologically, due to the restrictions made by regulators and governments. Water pipes based on lead (Pb) was rumoured to have beleaguered the Roman empire and led to its downfall, can be a debatable topic but it is an established fact that the tap water in ancient Rome was found to possess 100 times more Pb than the local spring water. Due to the dissolvability character of lead, it imposes great threat to our planet, where since 1970 Pb usage is highly regulated and being minimized. Lead compounds are known to be very toxic and harmful to the environment, and its application can trigger the environmental pollution.^[1b] Its hazards to health and the risks associated are very high and less than 10 ppm in human blood can impose threat to life.^[2-4] The usage of lead shows serious hazard to health and environment^[5] and prolonged exposure is carcinogenic, toxic to aquatic life moreover it can pass to baby through breast-feeding. For such reason its usage is restricted, controlled by harmonised classifications and labelling's and is strictly regulated in many countries. The most investigated perovskite material for solar cells application is methylammonium lead triiodide (MAPbI₃), which converts back into PbI₂ upon water absorption (through atmosphere).^[6-8] It is expected for a wide scale acceptability and consensus building across the political table, it is paramount to develop materials, which are lead free. The scrutiny of harmful PV material allowed the

scientific community to design green candidates, which can harvest light effectively at cut rate price for thin film PV. For wide scale deployment identification of ideal absorber, which are lead free and shows panchromatic light absorption, will make this technology closer to commercial endeavour. Recently, by the use of multi-cation and anion, inclusion of hydrophobic moieties through compositional engineering of perovskites, spacer layer incorporation and insertion of larger cation to produce Ruddlesden–Popper phase in perovskites has been adopted to address stability issues. It is beyond the scope of the present review to comment about the Ruddlesden–Popper phase, which in recent literatures are termed as 2-dimensional perovskites. Ideally, 2D Materials are those materials, which has sheets thinner than the Fermi wavelength (or De Broglie wavelength), which is not the case with perovskites. We direct the reader to a recent commentary for further clarification on terminology for dimensionality in perovskites.^[1c] However, the lead (Pb) toxicity can be mitigated by adopting the strategies such as the use of divalent, trivalent or tetravalent cations in perovskite for Pb substitution or by employing metal-deficient iodosalts and dimer structure. The opportunity to predict new composition, which is Pb-free mainly relies on playing with different combinatorial approach, however the presence of large number of variants makes the task demanding. Figure 1a and b illustrate the schematic of the crystal structures of Pb perovskites and lead-free perovskite. The replacement of Pb with new divalent cations, such as transition metals was also explored.^[9,10] Different research directions were undertaken to change the composition space in ABX₃ perovskite materials. Existence of metal deficient, double perovskites, and multidimensional perovskites with complete or partial substitutions in the perovskite structure may suggest an astonishing combination^[11] number of 10⁴-10⁶. Here, we have summarized the approaches, which is centred around to overcome one of the most daunting challenges in Pb halide based PSCs, i.e the replacement of toxic lead (Pb) with other eco-friendly candidates in the perovskite structure. Closing the gap between high efficiency, and long lifetimes by eliminating toxic materials is a remarkable challenge and new lead-free perovskite materials can play an important role to achieve these ambitious goals. Recently, several groups have made attempts to elucidate and understand the underlying phenomena behind the Pb replacement trend in perovskite materials, including CH₃NH₃SnI₃,^[12] CH₃NH₃CuX₄,^[13] (CH₃NH₃)₂MnCl₄,^[14] AGeI₃ (A = inorganic or organic cation, such as Cesium (Cs), methyl ammonium (MA), or formamidinium cation (FA))^[9]. Its tin analogues CH₃NH₃SnI₃ and CsSnI₃ have shown potential in terms of electrical properties, but they are highly sensitive to the oxygen and their tolerance behaviour to moisture is relatively poor.

2. The quest of Pb-Free Perovskite Solar Cells (PSCs)

The results obtained at lab scale from PSCs depending on lead (Pb) materials show high performance; however, assembly and disposal of these kind of PSCs are harmful to the environment due to the high toxicity of Pb. It is of paramount importance to overcome such environmental barrier, in order to make our planet clean. The advent of eco-friendly light harvester is the mission to obviate the pollution problems and to expand their applications. Metal substitution of lead with non-toxic metal to form a lead-free perovskite is pre requisite for a green and clean world.

The policy makers and regulators reluctance, intriguing a great deal of interest by replacing lead with nontoxic metals such as tin, bismuth, and germanium.^[17–19]

2.1 Substitution at the B site using divalent metal cations: Divalent substitution

2.1.1 Sn-based lead-free PSCs

The emergence of the layered perovskites (Ruddlesden–Popper phase) was envisioned to address the long-term instability issue in the traditional 3D perovskite; layered perovskites also has intrinsically remarkable electronic and optical characteristics and are considered as derivatives of the 3D perovskites. Here, 3D frameworks are sliced into well-defined 2D slabs.^[17–20] In terms of composition, such Ruddlesden–Popper phase perovskites have the generic formula of $(\text{RNH}_3)_2(\text{A})_{n-1}\text{MX}_{3n+1}$ (here n is an integer), RNH_3 is a primary aliphatic or aromatic alkylammonium cation, A and M are cations, and X represents an anion like their 3D counterparts. In 2D network containing the inorganic perovskite layers of the corner-sharing $[\text{MX}_6]_4$ octahedron is confined between interdigitating bilayers of long-chain alkylammonium cations that act as a spacer between the perovskite layers. Tin (Sn) was emerged as the first possible candidate from group 14 elements with comparable ionic radii to replace lead (Pb) in the perovskite structure for solar cells fabrication. The initial attempt was followed by the deployment of other elements from the periodic table, as potential candidates for Pb replacement and are represented in Figure 2a. The presence of similar physical properties of tin based perovskites as of lead, was aim to achieve similar electrical performance, Sn based perovskites suffer from p-doping which in turn increases the carrier density in dark and limits the photo-generated properties.^[20] In the first report of tin-based PSCs, PCE of 6% was achieved.^[21,22] This was further optimized to allow improvements in tin-based PSCs performance.^[23] Though, tin-based perovskite such as methylammonium tin iodide (MASnI_3), formamidinium tin iodide (FASnI_3), or Cesium tin iodide (CsSnI_3) possesses ideal band gap (1.2–1.4 eV) along with high carrier mobility, but they suffer from low stability and conductivity due to the oxidation of Sn^{2+} to Sn^{4+} .^[24] The partial substitution of Pb was also adapted to form $\text{CH}_3\text{NH}_3\text{Sn}_x\text{Pb}_{1-x}\text{I}_3$,^[25,26] and it was found that by increasing the Sn concentration, band gap can be narrowed. The first report on lead-free PSCs based on $\text{CH}_3\text{NH}_3\text{SnI}_3$ was reported the PCE of 5.23%^[10] and 6.4%^[27], with the suppression of Sn^{4+} formation by using ultrahigh purity precursors materials, careful and controlled synthetic conditions. $\text{CH}_3\text{NH}_3\text{SnI}_3$ (MASnI_3) possesses favourable band gap which is near to the ideal Shockley–Queisser value^[28] (Figure 2b). Correspondingly, Snaith et al. has investigated the crystal structure of MASnI_3 (Figure 2 c and d), and the device structure is represented in Figure 2e. The obtained results were in agreement with simulated and literature data, and corresponds to the tetragonal conformation of the perovskite structure.^[29, 30] Maximum PCE reported were based on compositional engineered (Sn and Pb ratio) perovskite yielded 7.37% for $\text{CH}_3\text{NH}_3\text{Sn}_{0.25}\text{Pb}_{0.75}\text{I}_3$. The addition of Pb ions help to retard oxidation of Sn^{2+} to Sn^{4+} as well as allow carrier concentration increase and thus higher PCE.^[26] However, the PCE of tin-based PSCs remains lower than that of lead-halide based PSCs, and additionally it was plagued by its fast degradation with moisture exposure. It is of utmost importance to develop new methods to improve the performance and importantly, the

stability for Sn-based perovskites, by optimizing its intrinsic properties. Qiu et al.^[31] reported B- γ -CsSnI₃ as light harvester, which spontaneously converts into an air-stable Cs₂SnI₆ film in air at room temperature. The growth of Cs₂SnI₆ film from CsSnI₃ via a two-step deposition method based on solid-state reaction as well as the crystal structures of Cs₂SnI₆ and CsSnI₃ are reported meticulously for details.^[35a] Additionally, Yan and co-workers studied the effect of passivation for air stable tin-based solar cells.^[35b] They presented hydroxybenzene sulfonic acid or its salt as an antioxidant additive inside the perovskite precursor solution along with excess SnCl₂. They suggested that the interaction between the sulfonate group and the Sn²⁺ ion enables the *in-situ* encapsulation of the perovskite grains with SnCl₂-additive complex layer and resulted in enhanced oxidation stability of the perovskite film. The authors found that their PSCs are able to maintain 80% of the efficiency over 500 h upon air exposure without encapsulation, which is over ten times longer than the best result reported previously. Moreover, Liu et al. focused in the fabrication of tin-based films with high coverage and improved aggregation in order to enhance the efficiency of the PSC.^[35c] They used two different methodology to increase the film coverage as well as average crystallite size in order to prevent electrical shunting in the fabricated devices.

The carrier diffusion length through broadband (Vis-NIR) and transient absorption for the excited-state dynamics of MASnI₃ through photo physics in these films was realized. The carrier recombination of MASnI₃ obeys the second-order recombination; this causes decay in kinetics of transient absorbance spectra and time-resolved fluorescence (TRF) emission of the material. Figure 3a represents the Vis-NIR transient absorbance spectra of a MASnI₃, spectral red shift using a 420–1600 nm probe pulse. There are four main features in the transient absorbance spectra: i) a pronounced ground state bleaching at 920 nm (1.35 eV), which is close to the optical bandgap 1.30 eV,^[17] ii) a relatively weak bleaching feature at 710 nm; iii) a photo-induced absorption band at 800 nm; and iv) a photo-induced absorption band at 630 nm.^[36] To obtain a judicious kinetic fit, a second-order recombination model was used, which was fitted as used to recover of the transient absorbance signal (ground state bleaching and photo-induced absorption) through the recombination of photo-generated free carriers rather than excitons. The species-associated with spectra and kinetics reconstructed from the overall fits are presented in Figure 3b and c. The results suggest that the calculated electronic structure of MASnI₃ arises from its very low excitons binding energy, which attributes to free carriers. Moreover, transient absorbance spectra of the MASnI₃ as a function of probe wavelength can be represented like pseudo-colour (ΔA) with clear trend towards blue shift by increasing excitation photon energy. In addition, hot carrier absorption shows pronounced photo-induced absorption band at 730 nm when the excitation photon energy is well above band gap (e.g., λ_{exc} = 430 and 600 nm). The excitation energy dependence of the transient absorbance spectra suggest the hot carrier relaxation model, used for the analyses of the transient absorbance spectra. In depth, ultrafast optical spectroscopy elucidating properties such as low surface recombination velocity as well as long minority carrier diffusion length are desirable attributes for understanding the mobility of excitons in CsSnI₃. Initially, black CsSnI₃ ingot with smooth surface, free of grain boundaries across a large area was obtained at room temperature in orthorhombic crystal structure (Figure 3e inset).^[37] The

photoluminescence (PL) spectra of CsSnI₃ show red shift between the peak founded at 950 nm (1.31 eV) for one photon excitation (400, 700 and 800 nm) and the other one founded at 990 nm (1.25 eV) for two photon excitation (1350 nm). This shift arises from PL re-absorption effect (e.g., high sub gap absorption from tail states; small Stokes shift),^[38-40] and to a smaller bandgap in the bulk crystal due to reduced lattice strain.^[41-43] To investigate the excitation-wavelength-dependent PL dynamics in CsSnI₃, photo-excited carrier concentrations was kept to $<4 \times 10^{17} \text{ cm}^{-3}$ to ensure dominant first-order recombination kinetics. The pseudo colour images of the TRPL profiles were discussed, and a lifetime lengthening with increasing excitation wavelengths was observed (Figure 3d).^[44, 45]

2.1.2 Ge-based lead-free PSCs

Germanium (Ge²⁺) was probed as an attractive candidate from group 14 in the periodic table for lead free perovskite formulation. Cai et al. succeeded to predict the electronic structure of CH₃NH₃GeI₃ (MAGeI₃) theoretically and reported its mobility, tuneable band gap (1.35 eV to 2.5 eV) and optical performance.^[46] At room temperature MAGeI₃ forms a distorted octahedron with C_m space group symmetry. Due to the incompatible Ge-I bond formation; the octahedral GeI₆⁻ is highly distorted. In MAGeI₃ optimized structure, each Ge atom coordinates to six (I) atoms, with four I atoms in the equatorial direction and two I atoms in the apical directions. The dipolar organic cations CH₃NH₃⁺ are situated at the corner of octahedron GeI₆⁻. MAGeI₃ has suitable band gap, high carrier mobility and absorption coefficients, and its tuneable charge transport properties will pave way of using such materials as either p type or n type semiconductor for PV application. Recently,^[47] the rhombohedral structure of CsGeX₃ (X = Cl⁻, Br⁻, I⁻) absorber was reported for PV application and its proposed crystal structure is shown in Figure 4a. The maximum PCE reported was 4.94% for CsGeX₃, ($J_{sc} = 18.78 \text{ mA cm}^{-2}$ and $V_{oc} = 0.52 \text{ V}$), which was significantly below the performance of MAPbI₃; but with a band gap similar to their Pb counterparts (~1.6, ~2.3, and ~3.1 eV for I⁻, Br⁻, and Cl⁻, respectively) to suggest competitive performance.^[48,49] Preparation of inorganic (Cs) or alternative hybrid perovskites using methylammonium (MA) and formamidinium (FA) organic cation as A⁺ cation position in germanium halide perovskite (AGeI₃) for solar cells was reported by Mhaisalkar et al.^[9] For the evaluation of absorption of the germanium based perovskite, the Tauc plot indicates change in the compounds colours by increasing size of the A⁺ (Cs⁺, MA⁺ and FA⁺) cation in the structure as shown in Figure 4b.^[50] The estimated value of the bandgap derived from Tauc plots are 1.63, 2.0 and 2.35 eV for CsGeI₃, MAGeI₃ and FAGeI₃, respectively. Furthermore, the valence band (VB) as well as the conduction band (CB) energy levels were calculated using photoemission spectroscopy and the reported optical bandgap values, are -5.10, -5.2, and -5.5 eV (as VB) and -3.47, -3.2 and -3.15 eV (as CB) for CsGeI₃, MAGeI₃ and FAGeI₃, respectively, (Figure 4c). Owing to similar trend as of other metal halide systems, the replacement of Cs with MA and FA molecules can result in decrease valence band level.^[51-57] Subsequently, optical data and PV parameters of metal halide perovskites along with the respective device structures: Homovalent substitution of the B site (Pb²⁺) with divalent tin(Sn²⁺) or germanium(Ge²⁺) cation are summarized in Table 1.

2.2 Substitution at the B site using trivalent metal cations

2.2.1. Trivalent substitution by Antimony (Sb^{3+}) in PSCs

Elements of group-VA ($\text{M}^{3+} = \text{Bi}^{3+}$ and Sb^{3+}) in the periodic table with the same outermost s- electrons and the lone-pair ns^2 state of Pb^{2+} ions were explored as a suitable substitute for lead, in order to have similar PV performance.^[95-104] Chalcogenides (Sb_2S_3 and Sb_2Se_3) structures were widely used as the possible composition of Sb perovskite materials for PV applications and PCE as high as 6.6% was reported.^[97] MX_6 octahedra structure can't form in case of AMX_3 due to their higher (+3) oxidation state and subsequently $\text{A}_3\text{M}_2\text{X}_9$ structure emerge as the stable stoichiometry for PSCs.^[105-109] In a recent report; a mere PCE of 0.49% of methylammonium Sb-based PSCs was reported.^[98] The low level of crystallinity as well as existence of pinhole resulted in decrease short circuit current and was the possible reason for low PCE. Furthermore, another possible structure of Sb-based perovskite materials depend on cesium (Cs) cations with the formula of $\text{Cs}_3\text{Sb}_2\text{I}_9$ was studied.^[99] Though rubidium (Rb) can form a stable layer of $\text{Rb}_3\text{Sb}_2\text{I}_9$ for PSCs, it possesses some disadvantages of appropriate orientation along the planes of the desired structure.^[100] Chu et al. reported crystal structure of $\text{A}_3\text{Sb}_2\text{I}_9$ for Sb-based perovskite materials with MA^+ and Cs^+ as the cations for lead-free PSCs fabrication.^[110] The devices based on methylammonium antimony iodide ($(\text{CH}_3\text{NH}_3)_3\text{Sb}_2\text{I}_9$) yielded the maximum PCE of 2.04%. The crystal structure of the $\text{A}_3\text{Sb}_2\text{I}_9$, comprise of bi-octahedral anionic metal halide $(\text{Sb}_2\text{I}_9)_3$ -clusters, integrated in the perovskite composition and encompassed by MA^+ or Cs^+ cations (Figure 5a & b). Furthermore, they studied the crystal structure as well as the composition of the $\text{MA}_3\text{Sb}_2\text{I}_9$ and $\text{Cs}_3\text{Sb}_2\text{I}_9$ with and without the hydroiodic acid additive using X-ray diffraction (XRD) and X-ray photoelectron spectroscopy (XPS) experiments as shown in Fig. 6c & d, respectively. The maximum intensity peak appears at a 2θ value of 24.8° and 39.8° for MA and Cs cation for $\text{M}_3\text{Sb}_2\text{I}_9$ perovskite respectively. It was noted that the addition of hydroiodic acid enhances the crystallinity and phase purity largely; this can be deduced from the higher peak intensities observed (Figure 5c). The authors noted that the peaks have shifted to lower 2θ values with the addition of hydroiodic acid. The plausible reason for this can be due to the hydroiodic acid dopant, which imparts more iodine ions with a larger ionic radius, causing strain on the unit cell dimensions.^[111] Moreover, and the composition of different Sb-based perovskite containing multi cations were screened using photoelectron spectroscopy spectra and summarized in Figure 5d. All the elements inside the structure with different atomic ratios depend on the cation used and can be investigated and established. In addition, Hebig et al. characterized the antimony perovskite based on MA cation (Figure 6e).^[98] Homogeneous surface of the substrate with hexagonal-shaped crystals, which is in agreement with the expected crystal structure of $(\text{CH}_3\text{NH}_3)_3\text{Sb}_2\text{I}_9$ (Figure 5a), were obtained for the samples with more than $2 \mu\text{m}$ grain size as illustrated in the inset images of Figure 5e. The solar cells fabricated using Sb-based perovskite was deposited using the spin coating technique followed by anti-solvent dripping. Expectedly, Chu et al. reported that the higher performance were obtained for the devices, which were fabricated using hydroiodic acid dopant in the $\text{M}_3\text{Sb}_2\text{I}_9$.^[112] Following the previous investigation and having the device configuration of glass/ITO/PEDOT:PSS/Sb-perovskite/ $\text{PC}_{71}\text{BM}/\text{C}_{60}/\text{BCP}/\text{Al}$, the PV performance (Figures 5f and g) as well as Quantum

efficiency was reported (Figures 5 h and i). Varying molar ratios of (SbI₃: MAI) for MA₃Sb₂I₉ or (SbI₃: CsI) for Cs₃Sb₂I₉, with or without hydroiodic acid additive yielded different performance (PCE, EQE and integrated J_{sc}). Table 2 shows the optical data and PV parameters of metal halide perovskites (ABX₃) along with the respective device structures: heterovalent substitution of the B site (Pb²⁺) with trivalent Sb³⁺ and Bi³⁺ cation.

2.2.2. Trivalent substitution by Bismuth (Bi³⁺) in PSCs

Considerable attention was also given to bismuth based compounds, such as Bi₂CrFeO₆,^[133,134] bismuth triiodide (BiI₃),^[135] and A₃Bi₂I₉ perovskites (A = CH₃NH₃, Cs)^[105] as a light harvester. Specially, (CH₃NH₃)₃Bi₂I₉ with undersized-grained, and compact or porous nano-structured morphologies has received significant attention in PSCs, however the reported PCE remains low (0.01–0.42%).^[105,136–142] The notable reason behind the low PCE of such materials is their large bandgap (2.1 eV), which prevents the visible light absorption. Among the reported bismuth-based absorbers, (CH₃NH₃)₃Bi₂I₉ [MA₃Bi₂I₉] is the widely studied polymorph type. Owing to the trivalence state of Bi³⁺, the solid structure of MA₃Bi₂I₉ features two face-sharing 0D perovskite structure, which is constructed by the MA⁺ surrounded binuclear octahedral (Bi₂I₉)₃[–] clusters, contrasting to the 3D MAPbI₃ perovskite. Zhang et al. made efforts to tune the performance of such devices by improving (CH₃NH₃)₃Bi₂I₉ film quality using high–low vacuum deposition (HLVD) route through a novel two steps technique as (Figure 6a,) in order to extend the absorbance spectra.^[113] In this technique, firstly, TiO₂-coated based substrates were evacuated in a vacuum chamber, to be prepared for the evaporation of smooth and compact BiI₃. Then for the homogeneous conversion into (CH₃NH₃)₃Bi₂I₉, films were exposed for MAI–BiI₃ gas–solid reaction in a delicate middle-separated ceramic vessel that mounted in a low vacuum oven at 140–180 °C for less than 10 h. This was followed by annealing of the deposited materials in air to enhance the crystallinity and remove any residual of MAI in the (CH₃NH₃)₃Bi₂I₉. The architect of the fabricated device as well as the energy level diagram adopted is illustrated in Figure 6b. The solar cells were fabricated in mesoporous structure using the configuration Glass/FTO/dense-TiO₂/mesoporous-TiO₂/(CH₃NH₃)₃Bi₂I₉/Spiro-OMeTAD/Au. To confirm, the formation of pure hexagonal crystal structure of (CH₃NH₃)₃Bi₂I₉ with no residual of BiI₃ or MAI, the X-ray diffractograms were recorded and its represent the (CH₃NH₃)₃Bi₂I₉ patterns (Figure 6c) and the results were in agreement with the predicted one. The microstructures of (CH₃NH₃)₃Bi₂I₉ are represented in Figure 6 d and e with different magnifications. The fabricated (CH₃NH₃)₃Bi₂I₉ films through two-step HLVD pathway show hexagonal, smooth, compact and crossing-ridged oriented crystalline grains, which are pinhole free. To further gain insight of the fabricated solar cell and each layer used, the cross section field emission- scanning electron microscopy (FE-SEM) analysis were performed by Mali et al. as shown in Figure 6f.^[114] Another alternative for the bismuth based perovskite light-absorbing materials is Cs₃Bi₂I₉ (CsBI) structure. Bai et al. fabricated CsBI based PSCs using dissolution-recrystallization method.^[143]

Cs₃Bi₂I₉ (CsBI) polycrystalline layers were prepared through the deposition of CsI and BiI₃ mixture in DMF solvent atop of uniform dense TiO₂ layer by means of anti-solvent technique using spin-coating method, followed by

annealing to induce crystallization.^[144] A thin layer of $\text{Cs}_3\text{Bi}_2\text{I}_9$ nanosheets was formed with deprived microstructure and film quality, large grains size along with voids were also observed. Tang et al. fabricated $\text{CsBi}_3\text{I}_{10}$ based solar cells and Figure 6g illustrates the stepwise procedure. The $\text{CsBi}_3\text{I}_{10}$ layer was spun-coated from the precursor on glass substrates through a previously reported modified spin-coating process.^[145] To study the nature of the perovskite, the X-ray diffraction (XRD) patterns were recorded. As shown in Figure 6h, all the diffraction peaks can be readily ascribed to the rhombohedral structure of BiI_3 , with lattice constants $a = 0.75$ nm and $c = 2.07$ nm, and the hexagonal structure of $\text{Cs}_3\text{Bi}_2\text{I}_9$, with lattice constants $a = 0.84$ nm and $c = 2.1$ nm.

Not only the surface properties but also the spectral absorption of the prepared active layers are important factors affecting the performance of fabricated solar cells. The UV-visible spectral absorption of the BiI_3 and $\text{MA}_3\text{Bi}_2\text{I}_9$ thin films at wide range of wavelengths and the PL spectra of $\text{MA}_3\text{Bi}_2\text{I}_9$ film are shown in Figure 7a. The device PCE depends largely on the light harvester ability to absorb more amount of light and convert it to electricity. There are two possible ways to understand the absorption mechanism depending on the bandgap difference between $(\text{CH}_3\text{NH}_3)_3\text{Bi}_2\text{I}_9$ and BiI_3 as well as the light scattering effect materialize at the deposited layers. The relation between the band gap and scattering effect with the deposited layers was inversely proportional, which states, the small grain sized materials with small band gap can absorb and scatter more light at shorter wavelength.^[148,149] The bandgaps of the BiI_3 and $(\text{CH}_3\text{NH}_3)_3\text{Bi}_2\text{I}_9$ were estimated to be 1.77 and 2.15 eV, respectively. Furthermore, more information related to the electron transfer and lifetimes of hole and electron was recorded through PL decay spectra and the lifetimes fitted by single-exponential function are 0.78, 0.75, and 0.66 ns for bare $\text{MA}_3\text{Bi}_2\text{I}_9$, $\text{MA}_3\text{Bi}_2\text{I}_9/\text{PEDOT:PSS}$, and $\text{MA}_3\text{Bi}_2\text{I}_9/\text{C}_{60}$, (Figure 7b). The fermi level of BiI_3 and $(\text{CH}_3\text{NH}_3)_3\text{Bi}_2\text{I}_9$ as semiconductors was found in the centre of the bandgaps, which can migrate to form stable space charge region and band bending at the hetero interface,^[150,151] when these two materials combine in specific ratio to form the composites. The band bending phenomena can modify the absorption and scattering of light, which result in increased V_{oc} and PCE of the fabricated solar cells. To gain insight in the composition of Bi based perovskite, we assume $\text{Cs}_3\text{Bi}_2\text{I}_9$ belongs to 0-D dimer species and Figure 7a illustrates the surrounding of bioctahedral $(\text{Bi}_2\text{I}_9)_3^-$ clusters by Cs^+ cations. This material have similar band structure as of $\text{MA}_3\text{Bi}_2\text{I}_9$ with the band gap of 2.2 eV (Figure 7d).^[96,152] Further, several bismuth based perovskite structure like silver-bismuth-iodine ternary system with the cubic structure of AgBi_2I_7 having a band gap of 1.87 eV as shown in Figure 7 (e and f), has also find application in solar cells fabrication.^[147,153]

3. Substitution at the B site using mixed valence cations

Efforts have been laid to study the progress on lead-free PSCs from experimental and theoretical points of view. Nakajima and Sawada performed computational simulation through a systematic high-throughput way, prior to experimental studies with density functional theory,^[154a] and 11025 structures of hybrid perovskite were revealed using the parallel many-core (K) supercomputer. Substitute of lead in the standard 3D-AMX₃ hybrid perovskites by nontoxic elements, without compromising efficiency and stability is a disadvantage in the made attempts. Korbel

et al. provided a computational insight in this direction by considering all the halide perovskite compounds that can form stable AMX_3 structures. Among over 30,000 speculative perovskites, only lead, germanium, and tin based perovskites was expected to show promising PV properties, owing to their uniqueness in terms of opto-electrical properties.^[154b] The revealed materials include single and double perovskites of ABX_3 and $A_2BB'X_6$ forms, respectively. The most important part is B or BB' as the normal structure of perovskite contains Pb and the problems of toxicity comes from this part. Thus, the possible examples of this part to replace Pb can be Be; B; C; N; Mg; Al; Si; P; Ca; Sc; Ti; V; Cr; Mn; Fe; Co; Ni; Cu; Zn; Ga; Ge; As; Sr; Y; Zr; Nb; Mo; Tc; Ru; Rh; Pd; Ag; Cd; In; Sn; Sb; Ba; Hf; Ta; W; Re; Os; Ir; Pt; Au; Hg; Tl; Pb; or Bi. Innovative 51 low-toxic halide single and double perovskites as possible candidates for environmentally friendly PSCs can be obtained through the screening procedure of all the compounds present in the materials database. The ABX_3 type three-dimensional perovskite has been described in section 2 with the possible replacement of lead using other group 14 elements. Here, in this section, lead-free double perovskites will be discussed exhaustively along with their application in PV.

As theoretical predicted the possible candidates for lead replacement in the perovskite structure, we assume that there can be different combination between different elements in different groups of periodic table. The proposed environmentally friendly halide double perovskites have been classified under six families: group-14–group-14, group-13–group-15, group-11–group-11, group-9–group-13, group-11–group-13, and group-11–group-15 double perovskites in terms of optical and carrier transport properties as shown in Figure 8A and 8B. Subsequently, isoivalent substitution with the same divalent lead ions were used to obtain group-14–group-14 double perovskites materials, which have the similar valence isoelectronic of group-13–group-15 double perovskites. Here, two divalent lead cations are replaced by a monovalent group-13 cation and a trivalent group-15 cation. All the candidates of group-13–group-15 double perovskites have direct band gaps and small carrier effective masses. In addition, a mixture of monovalent B and trivalent B' metal cations forms the group-11–group-11 double perovskites.^[155] Further, no experimental or theoretical studies have yet been carried out for the direct band gaps group-9–group-13 double perovskites, which are valence-isoelectronic to the group-11–group-11 ones. Later, MA_2CuInI_6 was chosen as the best among the possible group-11–group-13 candidates due to its low cost fabrication. Moreover, most of group-11–group-15 materials were removed from the candidate list due to its indirect and large band gaps behaviour. These theoretical findings can be used as library of extensive materials database and provide guidance to experimentally validate these candidates, in order to put forward a new series of Pb halide perovskite materials.

3.1. Experimental validity of different split-cation dopants in Pb-free PSCs

Only few combinations of mixed valence cation as discussed above are found to be experimentally feasible. More specifically, group-14–group-14 and group-11–group-15 double perovskites were explored so far as described in detail in next section.

3.1.1. (Sn-Ge) [group-14–group 14] mixed cations double perovskite

The group-14-group-14 elements demonstrate an astonishing set of Pb-free semiconductor with a suitable energy band gap for efficient solar cells fabrication. Few research groups have focused on such kind of double perovskite based lead free materials such as (Sn-Ge) materials; which can be prepared in the similar fashion as of (Sn-Pb) in bication perovskite.^[156] An array of characterizations techniques were employed to confirm the structure of the acquired materials and check their ability as light harvester for PV application.

Sadhanala, et al. reported different molar ratios of the metal ion composition in (Sn-Ge) matrix and scrutinized the influence of structural geometry on the opto-electrical properties.^[157] The approach was based on the similar fashion as of (Sn-Pb) based perovskite and adopted the replacement of Pb with Ge in the Pb-Sn solid solutions and fabricated Sn-Ge mixed alloy by using single-step solution processing and vapour deposition methods. In a recent past, Ju et al. conceptualized the efficient behaviour of suitable band gap mixed Sn-Ge based perovskites like $\text{CsSn}_{0.5}\text{Ge}_{0.5}\text{I}_3$, $\text{CH}_3\text{NH}_3\text{Sn}_{0.5}\text{Ge}_{0.5}\text{I}_3$, $\text{Cs}_{0.5}(\text{CH}_3\text{NH}_3)_{0.5}\text{Sn}_{0.5}\text{Ge}_{0.5}\text{I}_3$, $\text{Cs}_{0.5}(\text{CH}(\text{NH}_2)_2)_{0.5}\text{Sn}_{0.5}\text{Ge}_{0.5}\text{I}_3$, and $\text{RbSn}_{0.5}\text{Ge}_{0.5}\text{I}_3$. In the case of $\text{RbSn}_{0.5}\text{Ge}_{0.5}\text{I}_3$ it was very similar to MAPbI_3 and expected to absorb light in a similar solar spectrum range.^[162] The crystal structure of perovskites based on germanium and tin solid solutions, $\text{CH}_3\text{NH}_3\text{Sn}_{(1-x)}\text{Ge}_x\text{I}_3$ ($0 \leq x \leq 1$), either in powder or thin film phase was established using different techniques. Thin film samples for the structures of MASnI_3 , $\text{CH}_3\text{NH}_3\text{Sn}_{0.75}\text{Ge}_{0.25}\text{I}_3$, $\text{CH}_3\text{NH}_3\text{Sn}_{0.50}\text{Ge}_{0.50}\text{I}_3$, $\text{CH}_3\text{NH}_3\text{Sn}_{0.25}\text{Ge}_{0.75}\text{I}_3$ and MAGeI_3 were studied using X-ray diffractograms and the patterns are illustrated in Figure 9a. Tetragonal phase was noted for MASnI_3 and MAGeI_3 perovskite. Additionally, the results show that displacement error either in the thin-film or powder based samples can cause monotonic shift in the lattice parameters peaks in the case of 50% Ge ion. Subsequently, a transition to the trigonal phase from the splitting of the tetragonal (111) and (012) peaks to the trigonal (003), (201), (113), and (211) peaks were noted for the 75% Ge powder sample.^[157] The authors concluded the structure was intact in the pure as well as mixed cases, where it has showed slight shift. The crystal structure of $\text{CH}_3\text{NH}_3\text{Sn}_{(1-x)}\text{Ge}_x\text{I}_3$ ($0 \leq x \leq 1$) is represented in Figure 9b. Further, for 50 % insertion of Ge into MASnI_3 results in an amplified spontaneous emission (ASE), which show narrowing of photoluminescence peak at higher excitation densities, reaching a FWHM value from ~ 75 nm to less than half ~ 40 nm. The band gap calculated from the normalized absorption spectra shows a monotonic shift of the band edge towards higher energy as a function of increase Ge content. By further measuring steady state PL and its decay (Figure 9 c and d), it was concluded that the 50% Ge based perovskite is an ideal candidate for diverse opto-electrical applications including solar cells, owing to its superior optical properties, suitable band gap and long charge-carrier recombination.

Another group, Hayase et al also focused on the Sn-Ge alloy based perovskite but as an alternative to MA cation, a mixture of MA and FA was used. They studied the structure of $\text{FA}_{0.75}\text{MA}_{0.25}\text{Sn}_{1-x}\text{Ge}_x\text{I}_3$ with different molar ratio of Sn-Ge alloy as a stable absorber layer for PSCs.¹⁵⁸ The preparation of the desired stoichiometry was made in a similar fashion as of other researchers and changing the molar ratio of $(\text{Sn}_{1-x}\text{Ge}_x; x = 0, 0.05, 0.1 \text{ and } 0.2)$.^[27,162] To predict the crystal structure of the materials, XRD patterns were recorded for the $\text{FA}_{0.75}\text{MA}_{0.25}\text{Sn}_{1-x}\text{Ge}_x\text{I}_3$. The hexagonal phase was observed for $\text{FA}_{0.75}\text{MA}_{0.25}\text{SnI}_3$ which shows peak around 14.5° and 28° , and on further doping with Ge

does not lead to appearance of any additional peak, suggesting the perovskite structure was not disrupted.^[163,164] However, the peak intensity at 14.5° and crystal size increases with doping of Ge. The optical properties of the perovskites with different (Sn-Ge) molar ratios are illustrated in Figure 9k and suggests remarkable optical properties, which vouch for its competitive performance in PV. Moreover, by examining the energy level diagram of these materials with different stoichiometry (Figure 9g), one can conclude that using these light harvesters in PSCs can improve the PV performance. For an optimized doping concentration of Ge (x=0.5), the PCE of 4.48% was achieved compared to un-doped FA_{0.75}MA_{0.25}SnI₃ perovskite, which yielded the PCE of 3.31 % (Figure 9f).

3.1.2. (Ag-Bi) [group 11–group 15] mixed cations double perovskite

The opportunity of combining two metals from different groups at B site for the cation part of double perovskite based materials can enhance the properties of the designed materials. Considering the case, if only one metal incorporates into the structure, it may change the behaviour and produce favourable materials with desired advantages. Thus, amalgamation of two different metals as Pb replacement in the hybrid perovskite structure will provide synergistic benefits of both metals and may result in astonishing materials for light harvesting. A new class of 3D metal perovskite hybrid structure has been investigated to provide rich substitutional lead-free light harvester double perovskites with promising opto-electrical features.^[165,166-171] Various research groups have characterized the crystal structure and made sincere efforts to understand the fundamental basis for series of double perovskite powders.^[172,166-167] Intrinsic features like suitable bandgap, high optical absorption coefficient, high stability and long carrier recombination lifetime enable Bi-based Cs₂AgBiBr₆ double perovskite semiconductor materials to be a potential candidate for PV application.^[166-168] Recently, researchers attempted to solve the challenge of fabricating high quality Cs₂AgBiBr₆ layers and thereafter solar cells using inverted configuration and obtained PCE close to 2.5%.^[173] Ning et al.^[175] was able to fabricate PSCs encompassing double perovskite using configuration of ITO/compact TiO₂/Cs₂AgBiBr₆/Spiro-OMeTAD/Au and evaluated its layer's structure by cross section FE-SEM (Figure 10 a & b). The cross-sectional micrograph confirms the formation of the layer by layer attached together uniformly with high crystallinity.^[174] Additionally, Wu et al. achieved high PCE using Cs₂AgBiBr₆ double perovskite materials as effective light harvester in the device fabrication.^[175]

Cs₂AgBiBr₆ powder with dark shining crystal and orange colour was dissolved in diverse polar solvents like dimethyl sulfoxide (DMSO) and was spun coated on the electrodes (substrate) utilizing anti-solvent approach to induce high crystallinity and probed as light harvester. The surface images of Cs₂AgBiBr₆ powder and solution as well as the surface roughness with root-mean-square (RMS) values are illustrated in Figure 10c. The Cs₂AgBiBr₆ was probed by XRD as well as surface FE-SEM analysis (Figure 10 d and e) and established its crystalline parameters. The materials showed promising behaviour as light harvester, which allowed the researchers to tweak the structure of solar cells, to further improve the PCE (Figure 10f).

Additionally, in order to understand the mechanism beyond the charge separation, transport and the operational property of PSCs, the band gaps of Cs₂BiAgCl₆ and Cs₂BiAgBr₆ double perovskite from experimental as well as

theoretical point were studied. These semiconductors reported to have indirect band gap through their electronic and optical measurements with (2.2-2.77) and (1.83-2.19) eV range values for $\text{Cs}_2\text{BiAgCl}_6$ and $\text{Cs}_2\text{BiAgBr}_6$, respectively.^[166,167,170]

From the theoretical point of view, diverse efforts were laid to calculate the band gap of these materials using density and hybrid functional theories.^[176-179] The bonding and antibonding states in both the valence and conduction bands with changes in the electronic structure of the two double perovskites with the halogen atom represented schematically in Figure 11a. The valence bandwidth depends on the halogen, by moving from Cl to Br, the energy of valence band increases and the width decreases. Hybridized Ag-d/halogen-p states are predominant throughout the highest valence band in both compounds, whereas the Ag-s states are pushed to the conduction band, consistent with the +1 character of the noble metal in this chemical environment. The top of the valence band show Bi-s/halogen-p antibonding state as illustrated in Figure 11b. Further, the spin-orbit coupling and splitting are the origin of isolated conduction and valence band, respectively, in band structure of both compounds, which caused splitting of the Bi- $p_{1/2}$ and Bi- $p_{3/2}$ states as illustrated in Figure 11 c & d. The results indicate that, the conduction band bottom in both cases has two minima, with energies within less than 0.2 eV. Subsequently, the conduction band bottom for either $\text{Cs}_2\text{BiAgCl}_6$ or $\text{Cs}_2\text{BiAgBr}_6$ founded at the Γ or L point, depending on whether calculations performed on the optimized or the experimental structures.^[180] The optical data and PV parameters of metal halide perovskites based solar cells along with the respective device structures: heterovalent substitution of the B site (Pb^{2+}) with double cation (Ag-Bi) and (Sn-Ge) are compiled in Table 3.

4. Substitution at B site by Transition metals

The rich chemistry and multiple oxidation state features of different transition metals such as Cu, Mn, Fe, Co, and Ni make them promising alternatives to Sn and Pb metals.^[186] Initial result of such materials in solution process PSCs reported by different groups, suggests the adaptability of transition metals, as substitute of lead and specifies the use of such structures for possible optimization. These advances validate that attractive PCE can be acquire by careful design and synthesis of matching sets of new Pb-free environmental friendly materials, in combination with improved device architectures and microstructure optimization. Using transition metal as possible replacement of Pb, can help minimizes the gap with the state of the art Pb based devices.

4.1. Cu-based lead-free PSCs

New approach in the layered perovskites by the copper usage, $(p\text{-F-C}_6\text{H}_5\text{-C}_2\text{H}_4\text{NH}_3)_2\text{CuBr}_4$ and $(\text{CH}_3(\text{CH}_2)_3\text{NH}_3)_2\text{CuBr}_4$ was reported employing low temperature solution based technique.^[193] However, these materials as light harvester in mesoscopic perovskite solar cells, yielded very low PCE of 0.51% and 0.63%, respectively.^[193] Up to now, three research groups have shown the use of copper in PSCs. Out of three reports, two of them focused on $(\text{CH}_3\text{NH}_3)_2\text{CuX}_4$ and investigate their properties as well as potential PV application. Mathews et al. reported a layered structure of $(\text{CH}_3\text{NH}_3)_2\text{CuCl}_{4-x}\text{Br}_x$ series, where the presence of Cl was founded to be vital for stabilization against Cu^{2+}

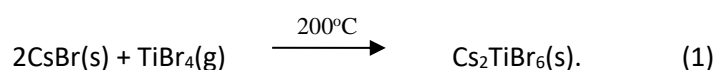
reduction.^[187] They claimed that the obtained materials with different molar compositions of Br/Cl ratios were crystalline. The characterized results for $(\text{CH}_3\text{NH}_3)_2\text{CuCl}_{4-x}\text{Br}_x$ set as XRD, UV-vis absorption and PL is shown in Figure 12 a-c and confirmed the encouraging properties of these materials for opto-electrical devices. The schematic diagram as well as the cross-section FE-SEM of $(\text{CH}_3\text{NH}_3)_2\text{CuCl}_2\text{Br}_2$ based solar cells is shown in Figure 12 d & e. To understand the science behind the electronic structure of the prepared materials, DFT calculation was made, which includes on-site Coulomb interactions (DFT+U) for this purpose. The $(\text{CH}_3\text{NH}_3)_2\text{CuCl}_4$ shows anti-ferromagnetic (AFM1) coupling with independent inorganic planes, which coinciding with previous electronic and magnetic studies.^[188] The predicted band gap energies of 3.09, 3.00, 2.88 and 2.86 eV for MA_2CuCl_4 , $\text{MA}_2\text{CuCl}_2\text{Br}_2$, $\text{MA}_2\text{CuClBr}_3$ and $\text{MA}_2\text{CuCl}_{0.5}\text{Br}_{3.5}$, respectively, interpreted from band structures as illustrated in Figure 12 g-j. The tuning of such materials band gap attributed to Br/Cl ratio, which tweak the absorption bands position. Figure 12f, depicts three different absorption bands for $\text{MA}_2\text{CuClBr}_3$, two are strong (1 and 2); which assigned to ligand-to-metal charge transfer (CT) transitions, as reported for CuCl_4^{2-} complexes,^[189] while the third band appear between 700 and 900 nm (3) was weak and assigned to d-d transitions within the d levels of Cu. This band shows no shift in absorption with the Br/Cl ratio variation across the series. The flat band structure of the holes can cause high and low effective masses along and in the Γ -Z direction, respectively (inset Figure 12 g-j) for different derived copper perovskites. This point towards, that the charge transport is favoured horizontally within the inorganic planes and hampered in the vertical direction.

The results obtained confirmed the homogeneity and high crystallinity of the designed materials together with the fine interface between the layers in the fabricated solar cell. This is vital for suitable pathway for the charges inside the cells and ideally suited for the light to electricity conversion process. Subsequently, Li et al.^[13] discussed the energy level diagram as well as schematic diagram of the lead free PSCs based on $(\text{CH}_3\text{NH}_3)_2\text{CuX}_4$ with different composition of Cl and Br (Figure 13 a and b). In a yet another study on Cu-based PSCs was focused on the perovskite to have dual function as absorber as well as hole transport materials. Wang et al. studied the PSCs with a structure of FTO/Compact $\text{TiO}_2/\text{TiO}_2\text{-ZrO}_2$ (immersed with perovskite)/Carbon layer, which emphasis the intimate contact between layers, enhance the charge movement, and yielded competitive PCE.^[190] The schematic as well as SEM cross section of the triple-layer, fully printable mesoscopic copper-based solar cell (Figure 13 c and d) shows that the mesoporous layers of TiO_2 and ZrO_2 were infiltrated with $\text{C}_6\text{H}_4\text{NH}_2\text{CuBr}_2\text{I}$ through the carbon layer printed on the top and have thicknesses of ~ 1 and $2 \mu\text{m}$, respectively. Figure 13e shows the excellent optical absorption behaviour of $\text{C}_6\text{H}_4\text{NH}_2\text{CuBr}_2\text{I}$ thin film, which cover the entire visible solar emission spectrum. Such a low PV performance of copper-based perovskites can be attributed to the high effective mass of holes, low absorption coefficient and inherent low conductivity of the 2D phase.^[193] Additionally, the composition of halides in these perovskites is another crucial factor as the halides play an essential part not only in tuning the optical gap of the perovskite but also in its stability. Introduction of bromide ions can reduce the band gap; they however promote

the partial reduction of Cu^{2+} to Cu^+ that affects the PCE by creating anion vacancies (electron traps). Chloride ions provide the essential stability against such undesired reduction of Cu^{2+} and improve the crystallinity. In order to achieve promising PCE with copper-based layered perovskites, it is paramount to address these concerns tactfully.

4.2. Ti-based lead-free PSCs

Another promising candidate from transition metal group for lead substitution was recently examined into the perovskite structure are titanium based materials. Titanium was introduced in the stoichiometry of Cesium titanium bromide (Cs_2TiBr_6) to develop promising materials suitable for solar cells applications. Padture et al. made seminal work on such kind of materials and they succeeded to deposit it and evaluated its performance in a PSCs.^[191] Various directions to improve Ti-based PSCs including the Cs_2TiBr_6 film-formation mechanisms as well as the PSCs device operation was reported. While Cs_2TiBr_6 consist of ($\text{CsBr} + \text{TiBr}_4$) in its composition, it can be fabricated easily through two steps vapour deposition technique as illustrated in Figure 14a. The uniform Cs_2TiBr_6 thin film deposited by mixing the two layers by depositing and annealing them together at selected temperature as illustrated in equation (1):



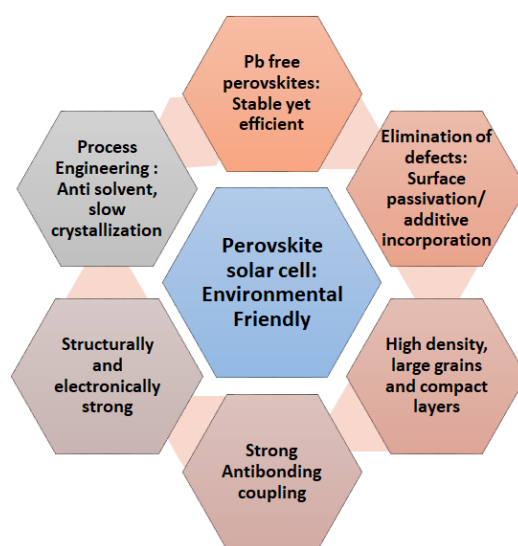
Further, three different type of thin films, were undertaken in this study and characterized using X-ray diffraction (XRD) methods. It was reported that XRD patterns peaks of these samples confirm the difference in crystallinity of each thin film, but they still validate the progression of equation (1) to form Cs_2TiBr_6 thin film. The opto-electrical properties of such newly developed compositional engineering perovskites based on as-prepared Cs_2TiBr_6 was evaluated to gauge the potential of these materials as a light harvester. The photoluminescence (PL) as well as Tauc plot of the Cs_2TiBr_6 thin film was recorded and no significant difference in the band gap of Cs_2TiBr_6 bulk powder and thin film (0.04 eV) was reported and the reported value was 1.78 and 1.82 eV for bulk and thin film, respectively.^[192] The excitation and emission wavelength values for Cs_2TiBr_6 thin film were 395 and 704, respectively for PL measurements, corresponding to the values of 1.76 eV that is reasonably bandgap. Further, the orderly PL intensity was suggested as the uniform physical features of the as-deposited Cs_2TiBr_6 thin films, which were highly consistent with the composition, phase, and microstructure results. In addition, PL decay dynamics considered as an important key to detect optoelectronic features of the prepared films through estimating the electron/hole diffusion lengths with and without quencher layers. Using the gained quenching decay results, they can estimate the charge-carrier diffusion length for electrons and holes in presence and in absence of either TiO_2 or P3HT as electron- and hole-quenching layers, respectively. The diffusion length data gave reasonable information to control the compositions of the light harvester and open the way towards the optimization of the microstructure of such materials for energy applications. A compact microstructure and pinhole-free CsBr , Cs_2TiBr_6 were obtained, and Cs_2TiBr_6 was sandwiched in a routine fashion between ETL and HTL to evaluate its PV performance. The preliminary results gave encouraging PCE in such a newly developed titanium substituted perovskites, and PCE of up to 3.3% was measured. The device

architecture adopted along with the corresponding energy-level diagram are illustrated in Figures 14b and 14c, respectively.

Summary and Future Perspective

The unprecedented results delivered by Pb-halide based perovskites in such a short time frame, is being plagued by the presence of environment and health toxic lead. Pb-free perovskite based light harvester are being put forward as a new era in the development of perovskite solar cells. The material intrinsic instability and the Pb toxicity issues are daunting challenge and requires significant attention to remove this barricade for its commercial endeavour. We aimed to address such challenges by suggesting criteria to choose Pb-free materials that has delivered competitive performance in solar cells and further elucidate the underlying electro-optical and physio-chemical properties. The understanding of the excited-state dynamics in Pb free perovskites is vital for its further optimization in device fabrication. Pb is heavy and dense metal; by virtue of this Pb^{2+} allows formation of a 3-dimensional symmetrical structure and its intrinsic electrical merits are owing to strong $6s|5p$ anti-bonding coupling. Using similar fashion to replace this, elements with ns^2 lone pairs, which form octahedral with halogen anions such as Sn^{2+} , Ge^{2+} , Bi^{3+} and Sb^{3+} are preferred candidates. Theoretical studies as well as experimental work by performing electro-optical characterization suggests comparable carrier lifetime and diffusion length in $MASnI_3$ as of $MAPbI_3$. However, Sn or Ge (Ge also has larger band gap) based perovskites found to be degrade faster than of Pb, strategies such as the usage of bilayer perovskites (Bi^{3+}/Sb^{3+}) to avoid phase transition caused by ion migration, delay in crystallization process, retard oxidation process through additive engineering or double perovskites formation can be adopted.

Here in, we have stressed the recent progresses on different possible crystal structure of these lead free materials, which categorized into ABX_3 , A_2BX_6 , $A_3B_2X_9$, and $A_2B^{1+}B^{3+}X_6$, systematically. Different metal cations such as Sn, Bi, Ge and Sb as an example of A_2BX_6 , $A_3B_2X_9$ category, Sn-Ge and Ag-Bi as an example of $A_2B^{1+}B^{3+}X_6$ category as well as transition metals like (Cu and Ti), were suggested so far as promising alternative for lead (Pb), which can be further tailored to meet the eco-friendly directions of the perovskite. Further, computational screening has expanded the fundamental studies of the currently synthesized Pb-free perovskites and can function as an elemental means for accelerating the innovation of competitive candidates. Most of double perovskites or transition metals based ones possesses relatively large bandgaps >1.8 eV, which is an undesirable feature of Pb-free perovskites and is not suitable for single junction photovoltaics applications. However, large band gap can be a positive feature for tandem cells. Besides, the continued endeavour for abundant composition selection of Pb-



free halide perovskites broadens the field of light harvesters and push the efficiency by accelerating the progress of the eco-friendly and cost-effective Pb-free perovskites solar cells through materials genome and device architects. Though sincere efforts were made to improve the overall power conversion efficiency, it is still significantly lower than those of Pb-based solar cells. The intrinsic issues need to be addressed to further improve the efficiency and stability, including enhancing material stability, exploiting new synthetic routes, designing suitable device structure, understanding photo-dynamics and underlying working mechanism. The future research direction points to the fundamental study of the physical properties of Pb-free halide perovskites to evaluate the potentiality of these emerging compounds comprehensively, with an aim to provide directives for upcoming materials and devices development. MAPbI₃, which enjoys the privilege to be widely investigated for solar cells application, and provided us remarkable knowledge, can be perceived as starting point to simulate and experimentally validate new Pb-free materials by materials genome to put forward a green and clean yet efficient perovskites for solar cells fabrication. The use of benign materials will inspire researchers and allow solving the humanity, one of the biggest challenge to provide affordable and clean energy.

Conflicts of interest

The authors declare no conflict of interest.

Acknowledgements

This work has received funding from the European Union H2020 Programme under European Research council Consolidator grant [MOLEMAT, [72630](#)].

References

- [1] a) http://www.nrel.gov/ncpv/images/efficiency_chart.jpg, **2016**. b) A. Reuben, J. D. Schaefer, T. E. Moffitt, J. Broadbent, H. Harrington, R. M. Houts, S. Ramrakha, R. Poulton, A. Caspi, *JAMA Psychiatry*, **2019**, doi:10.1001/jamapsychiatry.2018.4192. c) J. Breternitz, and S. Schorr, *Adv. Energy Mater.*, **2018**, *8*, 1802366.
- [2] A. E. Shalan, S. Narra, T. Oshikiri, K. Ueno, X. Shi, H.-P. Wu, M. M. Elshanawany, E. W.-G. Diau and H. Misawa, *Sustainable Energy & Fuels*, **2017**, *1*, 1533-1540.
- [3] C.-M. Tsai, N. Mohanta, C.-Y. Wang, Y.-P. Lin, Y.-W. Yang, C.-L. Wang, C.-H. Hung and E. W.-G. Diau, *Angew. Chem. Int. Ed.*, **2017**, *56*, 13819-13823.
- [4] C.-M. Tsai, H.-P. Wu, S.-T. Chang, C.-F. Huang, C.-H. Wang, S. Narra, Y.-W. Yang, C.-L. Wang, C.-H. Hung and E. W.-G. Diau, *ACS Energy Lett.*, **2016**, *1*, 1086-1093.
- [5] S. Kazim, M. K. Nazeeruddin, M. Grätzel, S. Ahmad, *Ang. Chem. Int. Ed.* **2014**, *53*, 2812-2824.
- [6] M. Salado, A. D. Jodlowski, C. R.-Carmona, G. de Miguel, S. Kazim, M. K. Nazeeruddin, S. Ahmad, *Nano Energy*, **2018**, *50*, 220-228.
- [7] A. N. El-Shazly, A. E. Shalan, M. M. Rashad, E. A. Abdel-Aal, I. .A. Ibrahim, M. F. El-Shahat, *RSC Advances*, **2018**, *8*, 24059-24067.

- [8] A. M. Elseman, A. E. Shalan, M. M. Rashad, A. M. Hassan, *Materials Science in Semiconductor Processing*, **2017**, *66*, 176-185.
- [9] T. Krishnamoorthy, H. Ding, C. Yan, W. L. Leong, T. Baikie, Z. Zhang, M. Sherburne, S. Li, M. Asta, N. Mathew, S. G. Mhaisalkar, *J. Mater. Chem. A*, **2015**, *3*, 23829-23832.
- [10] S. Korbøl, M. A. L. Marques, S. Botti, *J. Mater. Chem. C*, **2016**, *4*, 3157-3167.
- [11] A. J. Lehner, D. H. Fabini, H. A. Evans, C. A. Hébert, S. R. Smock, J. Hu, H. Wang, J. W. Zwanziger, M. L. Chabinyč, R. Seshadri, *Chem. Mater.*, **2015**, *27*, 7137-7148.
- [12] P. Umari, E. Mosconi, and F. De Angelis, *Sci. Rep.*, **2014**, *4*, 4467.
- [13] A. M. Elseman, A. E. Shalan, S. Sajid, M. M. Rashad, A. M. Hassan, and M. Li, *ACS Appl. Mater. Interfaces*, **2018**, *10*, 11699-11707.
- [14] Z. H. Nie, J. Yin, H. W. Zhou, N. Chai, B. L. Chen, Y. T. Zhang, K. G. Qu, G. D. Shen, H. Y. Ma, Y. C. Li, J. S. Zhao, and X. X. Zhang, *ACS Appl. Mater. Interfaces*, **2016**, *8*, 28187-28193.
- [15] L. Calio, S. Kazim, M. Gratzel, and S. Ahmad, *Angew. Chem. Int. Ed.* **2016**, *55*, 14522-14545.
- [16] F. Giustino, H. J. Snaith, *ACS Energy Lett.*, **2016**, *1*, 1233-1240.
- [17] F. Hao, C. C. Stoumpos, D. H. Cao, R. P. H. Chang, and M. G. Kanatzidis, *Nat. Photonics*, **2014**, *8*, 489.
- [18] J. Chen, S. Zhou, S. Jin, H. Li, and T. J. Zhai, *Mater. Chem. C*, **2016**, *4*, 11.
- [19] Q. Shen, Y. Ogomi, J. Chang, T. Toyoda, K. Fujiwara, K. Yoshino, K. Sato, K. Yamazaki, M. Akimoto, Y. Kuga, K. Katayama, and S. Hayase, *J. Mater. Chem. A*, **2015**, *3*, 9308-9316.
- [20] E. Jokar, C.-H. Chien, C.-M. Tsai, A. Fathi, and E. W.-G. Diau, *Adv. Mater.*, **2018**, *31*, 1804835.
- [21] C.-M. Tsai, Y.-P. Lin, M. K. Pola, S. Narra, E. Jokar, Y.-W. Yang, and E. W.-G. Diau, *ACS Energy Lett.*, **2018**, *3*, 2077-2085.
- [22] E. Jokar, C.-H. Chien, A. Fathi, M. Rameez, Y.-H. Changa and E. W.-G. Diau, *Energy Environ. Sci.*, **2018**, *11*, 2353-2362.
- [23] A. D. Jodlowski, C. R.-Carmona, G. Grancini, M. Salado, M. Ralaiarisoa, S. Ahmad, N. Koch, L. Camacho, G. D. Miguel, M. K. Nazeeruddin, *Nature Energy*, **2017**, *2*, 972.
- [24] A. E. Shalan, M. Rasly, I. Osama, M. M. Rashad, I. A. Ibrahim, *Ceramics International*, **2014**, *40*, 11619-11626.
- [25] Y. Ogomi, A. Morita, S. Tsukamoto, T. Saitho, N. Fujikawa, Q. Shen, T. Toyoda, K. Yoshino, S. S. Pandey, T. Ma, S. Hayase, *J. Phys. Chem. Lett.*, **2014**, *5*, 1004-1011.
- [26] F. Hao, C. C. Stoumpos, R. P. H. Chang, M. G. Kanatzidis, *J. Am. Chem. Soc.* **2014**, *136*, 8094-8099.
- [27] N. K. Noel, S. D. Stranks, A. Abate, C. Wehrenfennig, S. Guarnera, A. Haghighirad, A. Sadhanala, G. E. Eperon, S. K. Pathak, M. B. Johnston, A. Petrozza, M. L. Herza and H. J. Snaith, *Energy Environ. Sci.*, **2014**, *7*, 3061-3068.
- [28] W. Shockley, H. J. Queisser, *J. Appl. Phys.*, **1961**, *32*, 510-510.
- [29] C. C. Stoumpos, C. D. Malliakas and M. G. Kanatzidis, *Inorg. Chem.*, **2013**, *52*, 9019-9038.
- [30] A. E. Shalan, T. Oshikiri, S. Narra, M. M. Elshanawany, K. Ueno, H.-P. Wu, K. Nakamura, X. Shi, E. W.-G. Diau, H. Misawa, *ACS applied materials & interfaces*, **2016**, *8*, 33592-33600.
- [31] X. Qiu, B. Cao, S. Yuan, X. Chen, Z. Qiu, Y. Jiang, Q. Ye, H. Wang, H. Zeng, J. Liu, M. G. Kanatzidis, *Solar Energy Materials & Solar Cells*, **2017**, *159*, 227-234.
- [32] P. B. Pablo, A. Shweta, M. K. Teck, M. Nripan, and G. M. Subodh, *J. Phys. Chem. Lett.*, **2015**, *6*, 898-907.
- [33] C. Soumyo, and J. P. Amlan, *J. Mater. Chem. A*, **2018**, *6*, 3793-3823.
- [34] W. Ke, C. C. Stoumpos, I. Spanopoulos, L. Mao, M. Chen, M. R. Wasielewski, and M. G. Kanatzidis, *J. Am. Chem. Soc.*, **2017**, *139*, 14800-14806.

- [35] a) I. Chung, J.-H. Song, J. Im, J. Androulakis, C. D. Malliakas, H. Li, A. J. Freeman, J. T. Kenney, and M. G. Kanatzidis, *J. Am. Chem. Soc.*, **2012**, *134*, 8579–8587. b) Q. Tai, X. Guo, G. Tang, P. You, T.-W. Ng, D. Shen, J. Cao, C.-K. Liu, N. Wang, Y. Zhu, C.-S. Lee, and F. Yan, *Angew. Chem. Int. Ed.* **2019**, *58*, 806–810. c) J. Liu, M. Ozaki, S. Yakumar, T. Handa, R. Nishikubo, Y. Kanemitsu, A. Saeki, Y. Murata, R. Murdey, A. Wakamiya, *Angew. Chem. Int. Ed.* **2018**, *57*, 13221–13225.
- [36] L. Ma, F. Hao, C. C. Stoumpos, B. T. Phelan, M. R. Wasielewski, and M. G. Kanatzidis, *J. Am. Chem. Soc.*, **2016**, *138*, 14750–14755
- [37] I. Chung, B. Lee, J. Q. He, R. P. H. Chang, M. G. Kanatzidis, *Nature* **2012**, *485*, 486.
- [38] Y. Yang, D. P. Ostrowski, R. M. France, K. Zhu, J. van de Lagemaat, J. M. Luther, M. C. Beard, *Nat. Photonics* **2016**, *10*, 53.
- [39] Y. Yamada, T. Yamada, L. Q. Phuong, N. Maruyama, H. Nishimura, A. Wakamiya, Y. Murata, Y. Kanemitsu, *J. Am. Chem. Soc.*, **2015**, *137*, 10456.
- [40] H. Wang, K. S. Wong, B. A. Foreman, Z. Y. Yang, G. K. L. Wong, *J. Appl. Phys.*, **1998**, *83*, 4773.
- [41] W. Y. Nie, H. H. Tsai, R. Asadpour, J. C. Blancon, A. J. Neukirch, G. Gupta, J. J. Crochet, M. Chhowalla, S. Tretiak, M. A. Alam, H. L. Wang, A. D. Mohite, *Science*, **2015**, *347*, 522.
- [42] V. D’Innocenzo, A. R. S. Kandada, M. De Bastiani, M. Gandini, A. Petrozza, *J. Am. Chem. Soc.*, **2014**, *136*, 17730.
- [43] G. Grancini, S. Marras, M. Prato, C. Giannini, C. Quarti, F. De Angelis, M. De Bastiani, G. E. Eperon, H. J. Snaith, L. Manna, A. Petrozza, *J. Phys. Chem. Lett.*, **2014**, *5*, 3836.
- [44] B. Wu, H. T. Nguyen, Z. Ku, G. Han, D. Giovanni, N. Mathews, H. J. Fan, T. C. Sum, *Adv. Energy Mater.*, **2016**, *6*, 1600551.
- [45] B. Wu, Y. Zhou, G. Xing, Q. Xu, H. F. Garces, A. Solanki, T. W. Goh, N. P. Padture, and T. C. Sum, *Adv. Funct. Mater.*, **2017**, *27*, 1604818.
- [46] Y.-Q. Zhao, B. Liu, Z.-L. Yu, D. Cao, M.-Q. Cai, *Electrochimica Acta*, **2017**, *247*, 891–898.
- [47] C. Huang, X. C. Yan, G. Cui, Z. Liu, S. Pang, H. Xu, *Chinese Pat. Appl. CN201410173750*, **2014**, <http://www.google.com/patents/CN103943368A?cl=en>.
- [48] L.-J. Chen, *RSC Adv.*, **2018**, *8*, 18396.
- [49] C. C. Stoumpos and M. G. Kanatzidis, *Adv. Mater.*, **2016**, *28*, 5778–5793.
- [50] L.-y. Huang and W. R. Lambrecht, *Phys. Rev. B: Condens. Matter Mater. Phys.*, **2013**, *88*, 165203.
- [51] F. Hao, C. C. Stoumpos, D. H. Cao, R. P. H. Chang and M. G. Kanatzidis, *Nat. Photonics*, **2014**, *8*, 489.
- [52] M. H. Kumar, S. Dharani, W. L. Leong, P. P. Boix, R. R. Prabhakar, T. Baikie, C. Shi, H. Ding, R. Ramesh, M. Asta, M. Graetzel, S. G. Mhaisalkar and N. Mathews, *Adv. Mater.*, **2014**, *26*, 7122–7127.
- [53] T. M. Koh, K. Fu, Y. Fang, S. Chen, T. C. Sum, N. Mathews, S. G. Mhaisalkar, P. P. Boix and T. Baikie, *J. Phys. Chem. C*, **2014**, *118*, 16458.
- [54] G. Xing, N. Mathews, S. Sun, S. S. Lim, Y. M. Lam, M. Gratzel, S. Mhaisalkar and T. C. Sum, *Science*, **2013**, *342*, 344.
- [55] P. Docampo, J. M. Ball, M. Darwich, G. E. Eperon and H. J. Snaith, *Nat. Commun.*, **2013**, *4*, 2761.
- [56] S. Sun, T. Salim, N. Mathews, M. Duchamp, C. Boothroyd, G. Xing, T. C. Sum and Y. M. Lam, *Energy Environ. Sci.*, **2014**, *7*, 399.
- [57] T. Erdem and H. V. Demir, *Nat. Photonics*, **2011**, *5*, 126.
- [58] C. C. Stoumpos, L. Frazer, D. J. Clark, Y. S. Kim, S. H. Rhim, A. J. Freeman, J. B. Ketterson, J. I. Jang, M. G. Kanatzidis, *J. Am. Chem. Soc.*, **2015**, *137*, 6804

- [59] N. K. Noel, S. D. Stranks, A. Abate, C. Wehrenfennig, S. Guarnera, A.-A. Haghighirad, A. Sadhanala, G. E. Eperon, S. K. Pathak, M. B. Johnston, A. Petrozza, L.M. Herz, H. J. Snaith, *Energy Environ. Sci.*, **2014**, *7*, 3061-3068.
- [60] F. Hao, C. C. Stoumpos, R. P. H. Chang, M. G. Kanatzidis, *J. Am. Chem. Soc.*, **2014**, *136*, 8094.
- [61] T.-B. Song, T. Yokoyama, C. C. Stoumpos, J. Logsdon, D. H. Cao, M. R. Wasielewski, S. Aramaki, M. G. Kanatzidis, *J. Am. Chem. Soc.*, **2017**, *139*, 836.
- [62] F. Hao, C. C. Stoumpos, P. Guo, N. Zhou, T. J. Marks, R. P. H. Chang, M. G. Kanatzidis, *J. Am. Chem. Soc.*, **2015**, *137*, 11445.
- [63] T. Fujihara, S. Terakawa, T. Matsushima, C. Qin, M. Yahiro, C. Adachi, *J. Mater. Chem. C*, **2017**, *5*, 1121.
- [64] T. Yokoyama, D. H. Cao, C. C. Stoumpos, T.-B. Bin Song, Y. Sato, S. Aramaki, M. G. Kanatzidis, *J. Phys. Chem. Lett.*, **2016**, *7*, 776.
- [65] Y. Yu, D. Zhao, C. R. Grice, W. Meng, C. Wang, W. Liao, A. J. Cimaroli, H. Zhang, K. Zhu, Y. Yan, *RSC Adv.*, **2016**, *6*, 90248.
- [66] X. Liu, Z. Yang, C.-C. Chueh, A. Rajagopal, S. T. Williams, Y. Sun and A. K.-Y. Jen, *J. Mater. Chem. A*, **2016**, *4*, 17939– 17945.
- [67] T. Yokoyama, T.-B. Song, D. H. Cao, C. C. Stoumpos, S. Aramaki, M. G. Kanatzidis, *ACS Energy Lett.*, **2017**, *2*, 22.
- [68] M.-C. Jung, S. R. Raga, Y. Qi, *RSC Adv.*, **2016**, *6*, 2819-2825.
- [69] T. B. Song, T. Yokoyama, C. C. Stoumpos, J. Logsdon, D. H. Cao, M. R. Wasielewski, S. Aramaki, M. G. Kanatzidis, *J. Am. Chem. Soc.*, **2017**, *139*, 836-842.
- [70] S. J. Lee, S. S. Shin, Y. C. Kim, D. Kim, T. K. Ahn, J. H. Noh, J. Seo, S. I. Seok, *J. Am. Chem. Soc.*, **2016**, *138*, 3974-3977.
- [71] W. Liao, D. Zhao, Y. Yu, C.R. Grice, C. Wang, A.J. Cimaroli, P. Schulz, W. Meng, K. Zhu, R.-G. Xiong, Y. Yan, *Adv. Mater.*, **2016**, *28*, 9333-9340.
- [72] J. Xi, Z. X. Wu, B. Jiao, H. Dong, C. X. Ran, C. C. Piao, T. Lei, T. B. Song, W. J. Ke, T. Yokoyama, X. Hou, M. G. Kanatzidis, *Adv. Mater.*, **2017**, *29*, 1606964.
- [73] S. J. Lee, S. S. Shin, J. Im, T. K. Ahn, J. H. Noh, N. J. Jeon, S. I. Seok, J. Seo, *ACS Energy Lett.*, **2017**, *3*, 46-53.
- [74] Z. Zhao, F. Gu, Y. Li, W. Sun, S. Ye, H. Rao, Z. Liu, Z. Bian, C. Huang, *Adv. Sci.*, **2017**, *4*, 1700204.
- [75] W. Ke, C. C. Stoumpos, J. L. Logsdon, M. R. Wasielewski, Y. Yan, G. Fang, M. G. Kanatzidis, *J. Am. Chem. Soc.*, **2016**, *138*, 14998.
- [76] T. M. Koh, T. Krishnamoorthy, N. Yantara, C. Shi, W. L. Leong, P. P. Boix, A. C. Grimsdale, S. G. Mhaisalkar, N. Mathews, *J. Mater. Chem. A*, **2015**, *3*, 14996.
- [77] S. Shao, J. Liu, G. Portale, H.-H. Fang, G.R. Blake, G.H. ten Brink, L.J.A. Koster, M.A. Loi, *Adv. Energy Mater.*, **2018**, *8*, 1702019.
- [78] W. Ke, C. C. Stoumpos, M. Zhu, L. Mao, I. Spanopoulos, J. Liu, O. Y. Kontsevoi, M. Chen, D. Sharma, Y. Zhang, M. R. Wasielewski, M. G. Kanatzidis, *Sci. Adv.*, **2017**, *3*, e1701293.
- [79] D. H. Cao, C. C. Stoumpos, T. Yokoyama, J. L. Logsdon, T.-B. Song, O. K. Farha, M. R. Wasielewski, J. T. Hupp, M. G. Kanatzidis, *ACS Energy Lett.*, **2017**, *2*, 982.
- [80] M. Zhang, M. Lyu, J.-H. Yun, M. Noori, X. Zhou, N. A. Cooling, Q. Wang, H. Yu, P. C. Dastoor, L. Wang, *Nano Res.*, **2016**, *9*, 1570.
- [81] Y. Liao, H. Liu, W. Zhou, D. Yang, Y. Shang, Z. Shi, B. Li, X. Jiang, L. Zhang, L.N. Quan, R. Quintero-Bermudez, B. R. Sutherland, Q. Mi, E.H. Sargent, Z. Ning, *J. Am. Chem. Soc.*, **2017**, *139*, 6693-6699.

- [82] W. Ke, C. C. Stoumpos, I. Spanopoulos, L. Mao, M. Chen, M. R. Wasielewski, M. G. Kanatzidis, *J. Am. Chem. Soc.*, **2017**, *139*, 14800-14806.
- [83] X. Wang, T. Zhang, Y. Lou and Y. Zhao, *Mater. Chem. Front.*, **2019**, *3*, 365-375.
- [84] N. Wang, Y. Zhou, M.-G. Ju, H. F. Garces, T. Ding, S. Pang, X. C. Zeng, N. P. Padture, X. W. Sun, *Adv. Energy Mater.*, **2016**, *6*, 1601130.
- [85] K. P. Marshall, R. I. Walton, R. A. Hatton, *J. Mater. Chem. A*, **2015**, *3*, 11631.
- [86] D. Sabba, H. K. Mulmudi, R. R. Prabhakar, T. Krishnamoorthy, T. Baikie, P. P. Boix, S. Mhaisalkar, N. Mathews, *J. Phys. Chem. C*, **2015**, *119*, 1763-1767.
- [87] M. Walker, R. I. Walton and R. A. Hatton, *J. Mater. Chem. A*, **2017**, *5*, 21836-21845.
- [88] W. Li, J. Li, J. Li, J. Fan, Y. Mai and L. Wang, *J. Mater. Chem. A*, **2016**, *4*, 17104-17110.
- [89] S. Gupta, T. Bendikov, G. Hodes, D. Cahen, CsSnBr₃, *ACS Energy Lett.*, **2016**, *1*, 1028-1033.
- [90] K. P. Marshall, M. Walker, R. I. Walton, R. A. Hatton, *Nature Energy*, **2016**, *1*, 16178.
- [91] T. B. Song, T. Yokoyama, S. Aramaki, M. G. Kanatzidis, *ACS Energy Lett.*, **2017**, *2*, 897-903.
- [92] X. Qiu, Y. Jiang, H. Zhang, Z. Qiu, S. Yuan, P. Wang, B. Cao, *Phys. Status Solidi RRL*, **2016**, *10*, 587-591.
- [93] X. Qiu, B. Cao, S. Yuan, X. Chen, Z. Qiu, Y. Jiang, Q. Ye, H. Wang, H. Zeng, J. Liu, M.G. Kanatzidis, *Sol. Energy Mater. Sol. Cells*, **2017**, *159*, 227-234.
- [94] B. Lee, A. Krenselewski, S.I. Baik, D. N. Seidman, R. P. H. Chang, *Sustain. Energy Fuels*, **2017**, *1*, 710-724.
- [95] K. M. Boopathi, S. Raman, R. Mohanraman, F.-C. Chou, Y.-Y. Chen, C.-H. Lee, F.-C. Chang and C.-W. Chu, *Sol. Energy Mater. Sol. Cells*, **2014**, *121*, 35-41.
- [96] B.-W. Park, B. Philippe, X. Zhang, H. Rensmo, G. Boschloo and E. M. J. Johansson, *Adv. Mater.*, **2015**, *27*, 6806-6813.
- [97] Y. C. Choi, Y. H. Lee, S. H. Im, J. H. Noh, T. N. Mandal, W. S. Yang and S. I. Seok, *Adv. Energy Mater.*, **2014**, *4*, 1301680.
- [98] J.-C. Hebig, I. Kühn, J. Flohre and T. Kirchartz, *ACS Energy Lett.*, **2016**, *1*, 309-314.
- [99] B. Saparov, F. Hong, J.-P. Sun, H.-S. Duan, W. Meng, S. Cameron, I. G. Hill, Y. Yan and D. B. Mitzi, *Chem. Mater.*, **2015**, *27*, 5622-5632.
- [100] P. C. Harikesh, H. K. Mulmudi, B. Ghosh, T. W. Goh, Y. T. Teng, K. Thirumal, M. Lockrey, K. Weber, T. M. Koh, S. Li, S. Mhaisalkar and N. Mathews, *Chem. Mater.*, **2016**, *28*, 7496-7504.
- [101] A. M. Ganose, C. N. Savory and D. O. Scanlon, *Chem. Commun.*, **2017**, *53*, 20-44.
- [102] J. Zaleski, R. Jakubas, L. Sobczyk and J. Mróz, *Ferroelectrics*, 1990, *103*, 83-90.
- [103] C. Zuo and L. Ding, *Angew. Chem., Int. Ed.*, **2017**, *56*, 6528.
- [104] B. Vargas, E. Ramos, E. P´erez-Guti´errez, J. C. Alonso and D. Solis-Ibarra, *J. Am. Chem. Soc.*, **2017**, *139*, 9116-9119.
- [105] B. W. Park, B. Philippe, X. Zhang, H. Rensmo, G. Boschloo, E. M. Johansson, *Adv. Mater.*, **2015**, *27*, 6806-6813.
- [106] M. Leng, Z. Chen, Y. Yang, Z. Li, K. Zeng, K. Li, G. Niu, Y. He, Q. Zhou, J. Tang, *Angew. Chem. Int. Ed.*, **2016**, *55*, 15012-15016.
- [107] K. Yamada, H. Sera, S. Sawada, H. Tada, T. Okuda, H. Tanaka, *J. Solid State Chem.*, **1997**, *134*, 319-325.
- [108] J.-C. Hebig, I. Kühn, J. Flohre, T. Kirchartz, *ACS Energy Lett.*, **2016**, *1*, 309-314.
- [109] C. Zuo, L. Ding, *Angew. Chem. Int. Ed.*, **2017**, *56*, 6528-6532.
- [110] K. M. Boopathi, P. Karuppuswamy, A. Singh, C. Hanmandlu, L. Lin, S. A. Abbas, C. C. Chang, P. C. Wang, G. Li and C. W. Chu, *J. Mater. Chem. A*, **2017**, *5*, 20843-20850.
- [111] H.-S. Kim and N.-G. Park, *J. Phys. Chem. Lett.*, **2014**, *5*, 2927-2934.

- [112] P. Karuppuswamy, K. M. Boopathi, A. Mohapatra, H.-C. Chend, K.-T. Wong, P.-C. Wang, C.-W. Chu, *Nano Energy*, **2018**, *45*, 330–336.
- [113] Z. Zhang, X. Li, X. Xia, Z. Wang, Z. Huang, B. Lei, and Y. Gao, *J. Phys. Chem. Lett.*, **2017**, *8*, 4300–4307.
- [114] S. S. Mali, H. Kim, D.-H. Kim, and C. K. Hong, *Chemistry Select*, **2017**, *2*, 1578 – 1585.
- [115] X.-W. Tong, W.-Y. Kong, Y.-Y. Wang, J.-M. Zhu, L.-B. Luo, and Z.-H. Wang, *ACS Appl. Mater. Interfaces*, **2017**, *9*, 18977–18985.
- [116] K. M. Boopathi, P. Karuppuswamy, A. Singh, C. Hanmandlu, L. Lin, S. A. Abbas, C. C. Chang, P. C. Wang, G. Li, C. W. Chu, *J. Mater. Chem. A*, **2017**, *5*, 20843–20850.
- [117] P. C. Harikeśh, H. K. Mulmudi, B. Ghosh, T. W. Goh, Y. T. Teng, K. Thirumal, M. Lockrey, K. Weber, T. M. Koh, S. Li, S. Mhaisalkar, N. Mathews, *Chem. Mater.*, **2016**, *28*, 7496–7504.
- [118] C. T. Zuo, L. M. Ding, *Angew. Chem. Int. Ed.*, **2017**, *56*, 6528–6532.
- [119] A. Singh, K. M. Boopathi, A. Mohapatra, Y. F. Chen, D.G. Li, C.W. Chu, *ACS Appl. Mater. Interfaces*, **2018**, *10*, 2566–2573.
- [120] F. Jiang, D. Yang, Y. Jiang, T. Liu, X.G. Zhao, Y. Ming, B. Luo, F. Qin, J. Fan, H. Han, L. Zhang, Y. Zhou, *J. Am. Chem. Soc.*, **2018**, *140*, 1019–1027.
- [121] M. B. Johansson, H. M. Zhu and E. M. J. Johansson, *J. Phys. Chem. Lett.*, **2016**, *7*, 3467–3471.
- [122] M. Q. Lyu, J. H. Yun, M. L. Cai, Y. L. Jiao, P. V. Bernhardt, M. Zhang, Q. Wang, A. J. Du, H. X. Wang, G. Liu and L. Z. Wang, *Nano Res.*, **2016**, *9*, 692–702.
- [123] T. Singh, A. Kulkarni, M. Ikegami and T. Miyasaka, *ACS Appl. Mater. Interfaces*, **2016**, *8*, 14542–14547.
- [124] X. Q. Zhang, G. Wu, Z. W. Gu, B. Guo, W. Q. Liu, S. D. Yang, T. Ye, C. Chen, W. W. Tu and H. Z. Chen, *Nano Res.*, **2016**, *9*, 2921–2930.
- [125] H. Li, C. Wu, Y. Yan, B. Chi, J. Pu, J. Li and S. Priya, *ChemSusChem*, **2017**, *10*, 3994–3998.
- [126] C. X. Ran, Z. X. Wu, J. Xi, F. Yuan, H. Dong, T. Lei, X. He and X. Hou, *J. Phys. Chem. Lett.*, **2017**, *8*, 394–400.
- [127] S. S. Mali, H. Kim, D. H. Kim and C. K. Hong, *Chemistry Select*, **2017**, *2*, 1578–1585.
- [128] A. Kulkarni, T. Singh, M. Ikegami and T. Miyasaka, *RSC Adv.*, **2017**, *7*, 9456–9460.
- [129] M. Abulikemu, S. Ould-Chikh, X. H. Miao, E. Alarousu, B. Murali, G. O. N. Ndjawa, J. Barbe, A. El Labban, A. Amassiana and S. Del Gobbo, *J. Mater. Chem. A*, **2016**, *4*, 12504–12515.
- [130] Z. Zhang, X. Li, X. Xia, Z. Wang, Z. Huang, B. Lei, Y. Gao, *J. Phys. Chem. Lett.*, **2017**, *8*, 4300–4307.
- [131] C. Lan, J. Luo, S. Zhao, C. Zhang, W. Liu, S. Hayase, T. Ma, *J. Alloys Compd.*, **2017**, *701*, 834.
- [132] T. Li, Y. Hu, C. A. Morrison, W. Wu, H. Han, N. Robertson, *Sustain. Energy Fuels*, **2017**, *1*, 308.
- [133] R. Nechache, C. Harnagea, S. Li, L. Cardenas, W. Huang, J. Chakrabartty, F. Rosei, *Nat. Photonics*, **2015**, *9*, 61–67.
- [134] C. H. Nie, J. Y. Chen, Y. L. Bai, S. F. Zhao, *Materials Letters*, **2016**, *175*, 258–261.
- [135] A. J. Lehner, H. B. Wang, D. H. Fabini, C. D. Liman, C. A. Hebert, E. E. Perry, M. Wang, G. C. Bazan, M. L. Chabiny, R. Seshadri, *Appl. Phys. Lett.*, **2015**, *107*, 131109.
- [136] S. Öz, J. C. Hebig, E. Jung, T. Singh, A. Lepcha, S. Olthof, F. Jan, Y. Gao, R. German, P. H. van Loosdrecht, K. Meerholz, T. Kirchartz, S. Mathura, *Sol. Energy Mater. Sol. Cells*, **2016**, *158*, 195–201.
- [137] T. Singh, A. Kulkarni, M. Ikegami, T. Miyasaka, *ACS Appl. Mater. Interfaces*, **2016**, *8*, 14542–14547.
- [138] A. Kulkarni, T. Singh, M. Ikegami, T. Miyasaka, *RSC Adv.*, **2017**, *7*, 9456–9460.
- [139] M. Lyu, J.-H. Yun, M. Cai, Y. Jiao, P. V. Bernhardt, M. Zhang, Q. Wang, A. Du, H. Wang, G. Liu, L. Wang, *Nano Res.* **2016**, *9*, 692–702.
- [140] X. Zhang, G. Wu, Z. Gu, B. Guo, W. Liu, S. Yang, T. Ye, C. Chen, W. Tu, H. Chen, *Nano Res.*, **2016**, *9*, 2921–2930.

- [141] J. Huang, Z. Gu, X. Zhang, G. Wu, H. Chen, *Journal of Alloys and Compounds*, **2018**, 767, 870-876.
- [142] M. Kong, H. Hu, L. Wan, M. Chen, Y. Gan, J. Wang, F. Chen, B. Dong, D. Eder, S. Wang, *RSC Adv.*, **2017**, 7, 35549-35557.
- [143] F. Bai, Y. Hu, Y. Hu, T. Qiu, X. Miao, S. Zhang, *Solar Energy Materials and Solar Cells*, **2018**, 184, 15-21.
- [144] N. J. Jeon, J. H. Noh, Y. C. Kim, W. S. Yang, S. Ryu, S. I. Seok, *Nat. Mater.*, **2014**, 13, 897-903.
- [145] X.-W. Tong, Z.-X. Zhang, D. Wang, L.-B. Luo, C. Xie and Y.-C. Wu, *J. Mater. Chem. C*, **2019**, 7, 863-870.
- [146] C. Ran, Z. Wu, J. Xi, F. Yuan, H. Dong, T. Lei, X. He, and X. Hou, *J. Phys. Chem. Lett.*, **2017**, 8, 394-400.
- [147] Y. Kim, Z. Yang, A. Jain, O. Voznyy, G.-H. Kim, M. Liu, L. N. Quan, F. P. García de Arquer, R. Comin, J. Z. Fan, E. H. Sargent, *Angew.Chem. Int. Ed.*, **2016**, 55, 9586.
- [148] K. Zhu, N. R. Neale, A. Miedaner, A.J. Frank, *Nano Lett.*, **2007**, 7, 69-74.
- [149] M. Mishchenko, L. Travis, A. Laci, Cambridge University Press, New York, **2002**.
- [150] L.T. Quynh, C. N. Van, Y. Bitla, J. W. Chen, T. H. Do, W. Y. Tzeng, S. C. Liao, K. A. Tsai, Y. C. Chen, C. L. Wu, C. H. Lai, C. W. Luo, Y. J. Hsu, Y. H. Chu, *Adv. Energy Mater.*, **2016**, 6, 1600686.
- [151] L. T. Quynh, J. Luo, S. Zhao, C. Zhang, W. Liu, S. Hayase, T. Ma, *Journal of Alloys and Compounds*, **2017**, 701, 834-840.
- [152] K.-H. Hong, J. Kim, L. Debbichi, H. Kim, S. H. Im, *J. Phys. Chem. C*, **2017**, 121, 969.
- [153] Z. Xiao, W. Meng, D. B. Mitzi, Y. Yan, *J. Phys. Chem Lett.*, **2016**, 7, 3903.
- [154] a) T. Nakajima and K. Sawada, *J. Phys. Chem. Lett.*, **2017**, 8, 4826-4831. b) S. Korbel, M. A. L. Marques and S. Botti, *J. Mater. Chem. C*, **2016**, 4, 3157-3167.
- [155] S. F. Hoefler, G. Trimmel, T. Rath, *Monatsh. Chem.*, **2017**, 148, 795-826.
- [156] Z. Zhao, F. Gu, Y. Li, W. Sun, S. Ye, H. Rao, Z. Liu, Z. Bian, C. Huang, *Adv. Sci.*, **2017**, 4, 1700204.
- [157] S. Nagane, D. Ghosh, R. L. Z. Hoye, B. Zhao, S. Ahmad, A. B. Walker, M. S. Islam, S. Ogale, and A. Sadhanala, *J. Phys. Chem. C*, **2018**, 122, 5940-5947.
- [158] N. Ito, M. A. Kamarudin, D. Hirotani, Y. Zhang, Q. Shen, Y. Ogomi, S. Iikubo, T. Minemoto, K. Yoshino, and S. Hayase, *J. Phys. Chem. Lett.*, **2018**, 9, 1682-1688.
- [159] Y. Liao, H. Liu, W. Zhou, D. Yang, Y. Shang, Z. Shi, B. Li, X. Jiang, L. Zhang, L. N. Quan, R. Q.-Bermudez, B. R. Sutherland, Q. Mi, E. H. Sargent, and Z. Ning, *J. Am. Chem. Soc.*, **2017**, 139, 6693-6699.
- [160] G. R. Kumar, H. J. Kim, S. Karupannan, K. Prabakar, *J. Phys. Chem. C*, **2017**, 121, 16447-16453.
- [161] C. C. Stoumpos, L. Frazer, D. J. Clark, Y. S. Kim, S. H. Rhim, A. J. Freeman, J. B. Ketterson, J. I. Jang, M. G. Kanatzidis, *J. Am. Chem. Soc.*, **2015**, 137, 6804-6819.
- [162] M. G. Ju, J. Dai, L. Ma, X. C. Zeng, *J. Am. Chem. Soc.* **2017**, 139, 8038-8043.
- [163] J. H. Heo, M. H. Lee, M. H. Jang, S. H. Im, *J. Mater. Chem. A*, **2016**, 4, 17636-17642.
- [164] A. L. Patterson, *Phys. Rev.* **1939**, 56, 978-982.
- [165] I. N. Flerov, M. V. Gorev, K. S. Aleksandrov, A. Tressaud, J. Grannec, M. Couzi, *Mater. Sci. Eng., R* **1998**, 24, 81.
- [166] E. T. McClure, M. R. Ball, W. Windl, P. M. Woodward, *Chem. Mater.*, **2016**, 28, 1348-1354.
- [167] A. H. Slavney, T. Hu, A. M. Lindenberg, H. I. Karunadasa, *J. Am. Chem. Soc.*, **2016**, 138, 2138-2141.
- [168] M. R. Filip, S. Hillman, A. A. Haghighirad, H. J. Snaith, F. Giustino, *J. Phys. Chem. Lett.*, **2016**, 7, 2579-2585.
- [169] W. Ning, F. Wang, B. Wu, J. Lu, Z. Yan, X. Liu, Y. Tao, J. M. Liu, W. Huang, M. Fahlman, L. Hultman, T. C. Sum, F. Gao, *Adv. Mater.*, **2018**, 30, 1706246.
- [170] G. Volonakis, M. R. Filip, A. A. Haghighirad, N. Sakai, B. Wenger, H. J. Snaith, F. Giustino, *J. Phys. Chem. Lett.*, **2016**, 7, 1254-1259.
- [171] X. G. Zhao, D. Yang, Y. Sun, T. Li, L. Zhang, L. Yu, A. Zunger, *J. Am. Chem. Soc.*, **2017**, 139, 6718-6725.

- [172] G. Volonakis, A. A. Haghghirad, R. L. Milot, W. H. Sio, M. R. Filip, B. Wenger, M. B. Johnston, L. M. Herz, H. J. Snaith, F. Giustino, *J. Phys. Chem. Lett.*, **2017**, *8*, 772.
- [173] E. Greul, M. L. Petrus, A. Binek, P. Docampo, T. Bein, *J. Mater. Chem. A*, **2017**, *5*, 19972–19981.
- [174] A. E. Shalan, A. M. Elseman, M. Rasly, M. M. Moharam, M. L.-Cantu, M. M. Rashad, *RSC Advances*, **2015**, *5*, 103095-103104.
- [175] W. Gao, C. Ran, J. Xi, B. Jiao, W. Zhang, M. Wu, X. Hou, and Z. Wu, *ChemPhysChem*, **2018**, *19*, 1–6.
- [176] J. P. Perdew, K. Burke, M. Ernzerhof, *Phys. Rev. Lett.*, **1996**, *77*, 3865.
- [177] J. Paier, R. Hirschl, M. Marsman, G. Kresse, *J. Chem. Phys.*, **2005**, *122*, 234102.
- [178] J. Heyd, G. E. Scuseria, M. Ernzerhof, *J. Chem. Phys.*, **2003**, *118*, 8207–8215.
- [179] J. Heyd, G. E. Scuseria, M. Ernzerhof, *J. Chem. Phys.*, **2006**, *124*, 219906.
- [180] M. R. Filip, S. Hillman, A.-A. Haghghirad, H. J. Snaith, and F. Giustino, *J. Phys. Chem. Lett.*, **2016**, *7*, 2579–2585.
- [181] S. K. I. Turkevych, E. Ito, T. Urano, K. Yamada, H. Tomiyasu, H. Yamagishi, M. Kondo, S. Aramaki, *ChemSusChem*, **2017**, *10*, 3754-3759.
- [182] Y. Kim, Z. Yang, A. Jain, O. Voznyy, G. H. Kim, M. Liu, L. N. Quan, F. P. Garcia de Arquer, R. Comin, J. Z. Fan, E. H. Sargent, *Angew. Chem. Int. Ed.*, **2016**, *55*, 9586-9590.
- [183] M. Pan, H. Zhu, M. B. Johansson, E. M. J. Johansson, *ChemSusChem*, **2017**, *10*, 2592-2596.
- [184] C. Wu, Q. Zhang, Y. Liu, W. Luo, X. Guo, Z. Huang, H. Ting, W. Sun, X. Zhong, S. Wei, S. Wang, Z. Chen, and L. Xiao, *Adv. Sci.*, **2018**, *5*, 1700759.
- [185] T. C.-J. Yang, P. Fiala, Q. Jeangros, C. Ballif, *Joule*, **2018**, *2*, 1421–1436.
- [186] F. Sani, S. Shafie, H. N. Lim and A. O. Musa, *Materials*, **2018**, *11*, 1008.
- [187] D. Cortecchia, H. A. Dewi, J. Yin, A. Bruno, S. Chen, T. Baikie, P. P. Boix, M. Grätzel, S. Mhaisalkar, C. Soci, and N. Mathews, *Inorg. Chem.*, **2016**, *55*, 1044–1052.
- [188] P. Zolfaghari, G. A. de Wijs, R. A. de Groot, *J. Phys.: Condens. Matter*, **2013**, *25*, 295502.
- [189] S. R. Desjardins, K. W. Penfield, S. L. Cohen, R. L. Musselman, E. I. Solomon, *J. Am. Chem. Soc.*, **1983**, *105*, 4590–4603.
- [190] X. Li, X. Zhong, Y. Hu, B. Li, Y. Sheng, Y. Zhang, C. Weng, M. Feng, H. Han, and J. Wang, *J. Phys. Chem. Lett.*, **2017**, *8*, 1804–1809.
- [191] M. Chen, M.-G. Ju, A. D. Carl, Y. Zong, R. L. Grimm, J. Gu, X. C. Zeng, Y. Zhou, and N. P. Padture, *Joule*, **2018**, *2*, 558–570.
- [192] M.-G. Ju, M. Chen, Y. Zhou, H. F. Graces, J. Dai, L. Ma, N. P. Padture, and X. C. Zeng, *ACS Energy Lett.*, **2018**, *3*, 297–304.
- [193] X.-P. Cui, K.-J. Jiang, J.-H. Huang, Q.-Q. Zhang, M.-J. Su, L.-M. Yang, Y.-L. Song, X.-Q. Zhou, *Synth. Metals*, **2015**, *209*, 247-250.



Ahmed Esmail Shalan is currently a postdoctoral researcher at BCMaterials, UPV/EHU, Spain with Prof. Shahzada Ahmad group. He obtained his B.Sc. (2008) and M.Sc. (2012) in Materials Science from Ain Shams University and Central Metallurgical R&D Institute, Egypt and his PhD (2017) from Hokkaido University, Japan, with Prof. Hiroaki Misawa and collaboration of Prof. Eric Diau -NCTU- Taiwan. He obtained a DAAD fellowship in (i-MEET-FAU), Germany with Prof. Christoph Brabec (2011) a with a visit to CIN2, UAB, Spain. He has authored >30 articles in the area of physical chemistry and materials science.



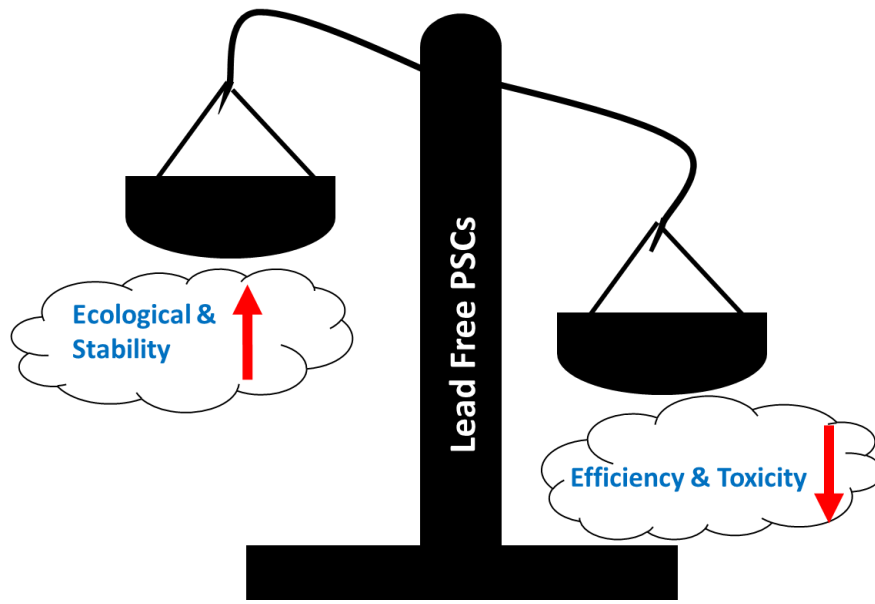
plasmonics for SERS.

Samrana Kazim is currently working as a group leader at Basque Centre for Materials, Applications and Nanostructures. Prior to this she has worked as a tenured Senior scientist (2013-2017) at a corporate research center of Abengoa. After finishing her Ph.D. in 2008 in Materials chemistry; she moved to Institute of Macromolecular Chemistry (IMC), Prague on IUPAC/UNESCO fellowship and subsequently as staff research scientist. She has competence in synthesis of metal nanoparticles and conducting polymers based nanocomposites. Her current research is focused on Designing, synthesis, and characterization of nanostructured materials, hybrid inorganic-organic solar cells, charge transport properties of organic semiconductor and,



Shahzada Ahmad is Ikerbasque professor; his scientific interests include materials for energy applications. He obtained his PhD degree in the field of materials science and moved to the Max Planck Institute for Polymer Research, to work on surfaces and interfaces by scanning probe microscopy. At EPFL, he developed nanoporous films for metal-free electro-catalysis and new redox shuttles. From 2012 to 2017 he was the program director of photovoltaics at Abengoa Research, a corporate research center. He is the inventor of patents and European research council consolidator grant awardee and among the cohort of distinguished scientists at the World Economic Forum.

TOC: Lead free materials for perovskite solar cells fabrication



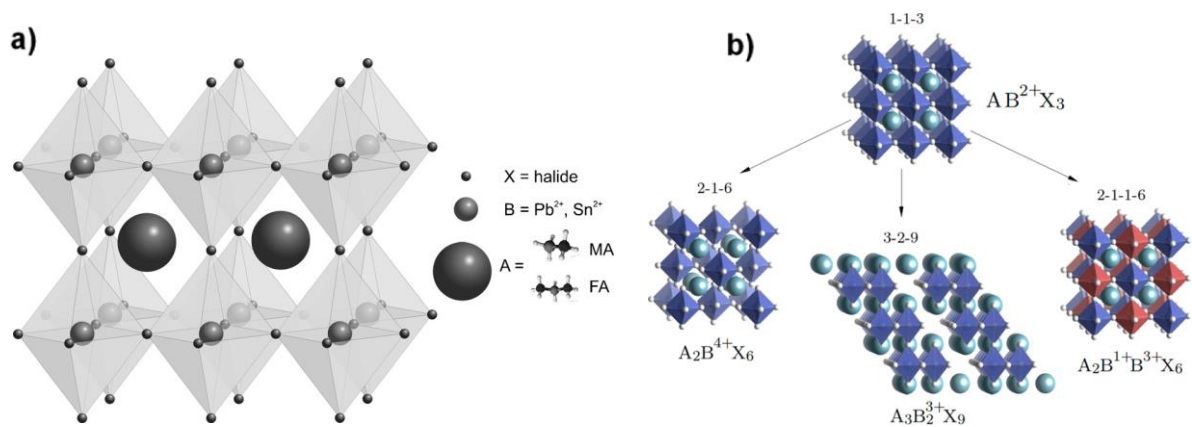


Figure 1 Schematic relation between the crystal structures of (a) Perovskite crystal structure and (b) lead-free perovskite derivatives. Reproduced with permission.^[15,16] Copyright 2016 Wiley-VCH & 2016 American chemical Society. Moving from left to right in right side (b), 2–1–6 compounds like Cs_2SnI_6 can be thought of as if obtained from lead halide perovskites by removing half of the B-site cations in a checkerboard pattern. In this case, charge neutrality requires the B-site cation to be in its +4 oxidation state. 3–2–9 compounds like $\text{Cs}_3\text{Sb}_2\text{I}_9$ can be imagined as derived from the perovskite at the top by removing one B-site cation every three, with all cations removed from planes defined by the $\langle 111 \rangle$ directions of the cubic perovskite crystal. In this case, the B-site cation must be in the +3 oxidation state in order to maintain charge neutrality. When the ionic radius of the A-site cation is large, the structure of these 3–2–9 compounds transforms into isolated facesharing bioctahedra, as in $\text{MA}_3\text{Sb}_2\text{I}_9$. 2–1–1–6 compounds like $\text{Cs}_2\text{BiAgCl}_6$ can be thought of as if obtained from the perovskite at the top by replacing every pair of adjacent B^{2+} cations by one B^{1+} and one B^{3+} cation, to define a rock-salt arrangement of cations.

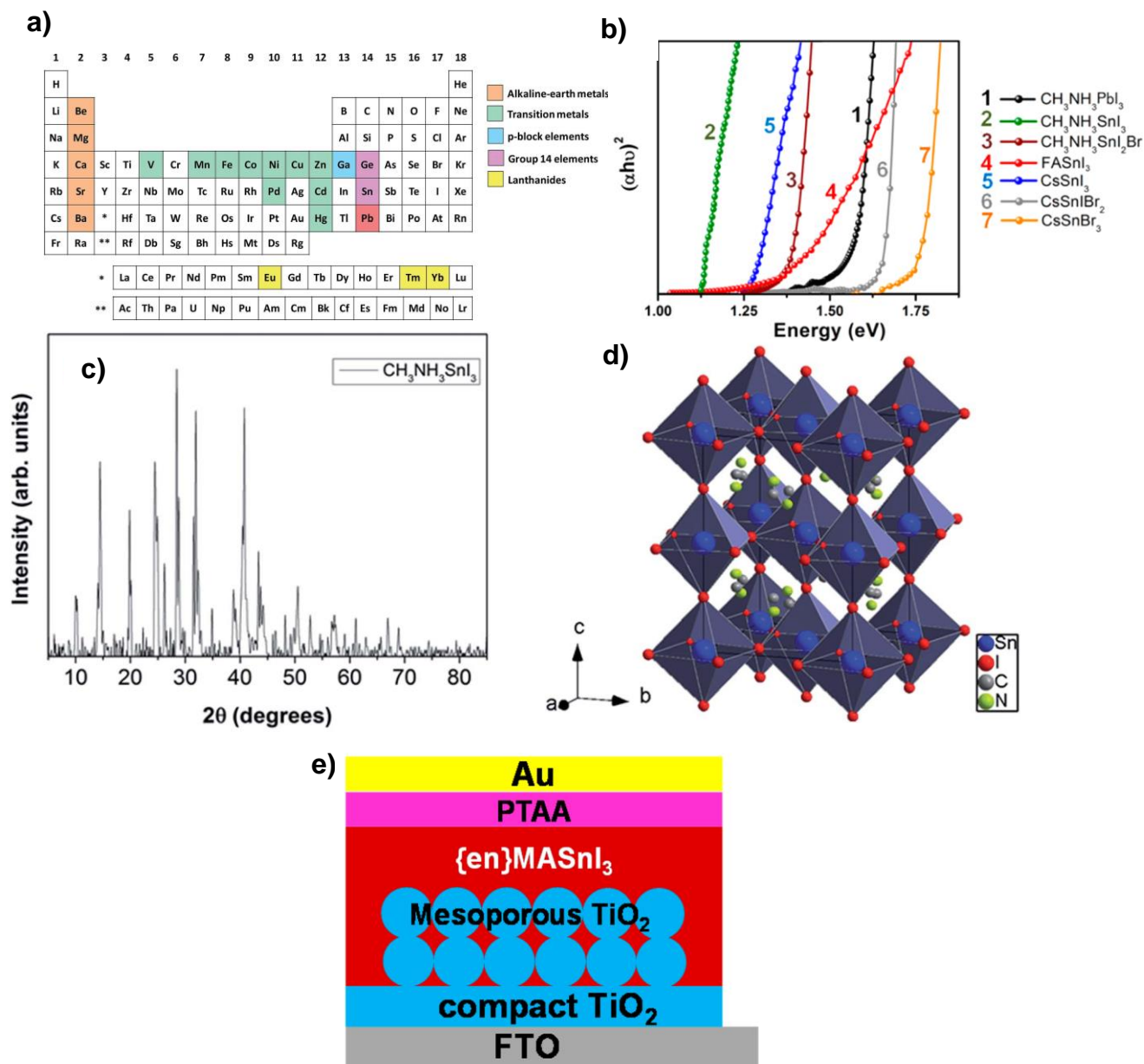


Figure 2 Metal substitution. **a.** Different elements from the periodic table of elements to replace lead in perovskites. Reproduced with permission.^[33] Copyright 2018 Royal Society of Chemistry. **b.** Tauc plots of several lead-free perovskites films compared with $\text{CH}_3\text{NH}_3\text{PbI}_3$ one. Reproduced with permission.^[32] Copyright 2015 American Chemical Society. **c.** X-ray Diffraction (XRD) pattern derived from a ground powder of $\text{CH}_3\text{NH}_3\text{SnI}_3$. **d.** Simulated crystal structure of $\text{CH}_3\text{NH}_3\text{SnI}_3$ obtained from the diffraction pattern given in (c) showing the tetragonal conformation of the perovskite lattice. Reproduced with permission.^[27] Copyright 2014 Royal Society of Chemistry. **e.** Solar cell structure of MASnI_3 . Reproduced with permission.^[34] Copyright 2016 American Chemical Society.

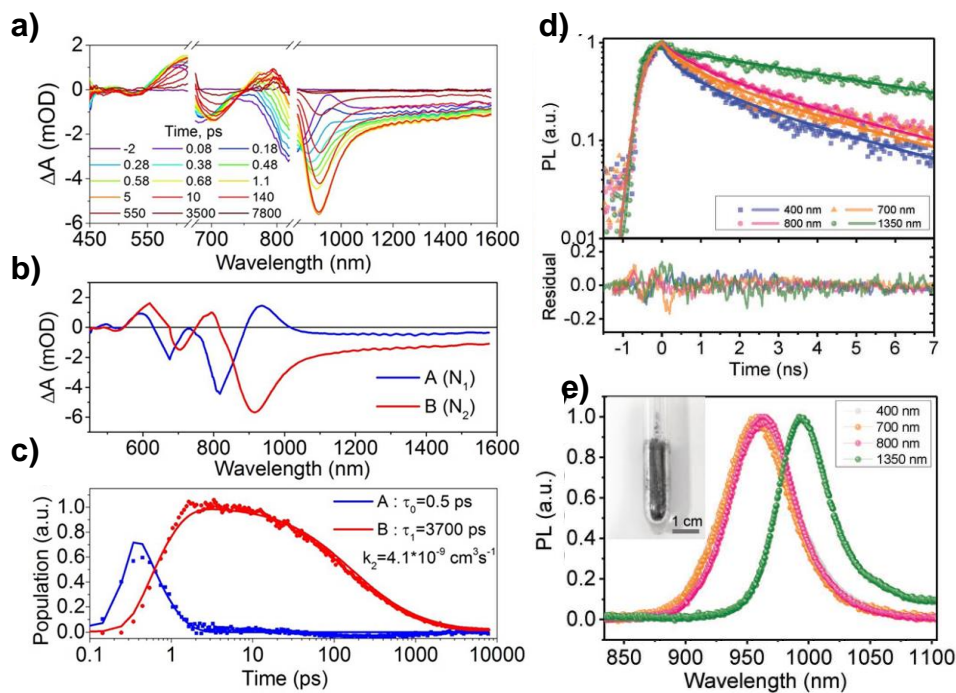


Figure 3. (a) Transient absorption spectra in the visible and NIR range under excitation at 650 nm at room temperature. The scattering from the pump (650 nm) and fundamental beam (830 nm) was removed for clarity. (b) Species-associated spectra and (c) kinetics reconstructed from the SVD global fit. Reproduced with permission.^[36] Copyright 2016 American Chemical Society. (d) Top: PL dynamics with different photoexcitation energies. Solid lines are fits using the model described in the main text. The carrier densities were kept low ($< 4 \times 10^{17} \text{ cm}^{-3}$) to ensure that first-order recombination dominates. Bottom: fitting residuals. (e) PL spectra of CsSnI₃ with one-photon (400, 700, and 800 nm) and two-photon (1350 nm) excitations. Inset: Photograph of CsSnI₃ ingot inside an evacuated Pyrex vial. Reproduced with permission.^[45] Copyright 2017 Wiley-VCH.

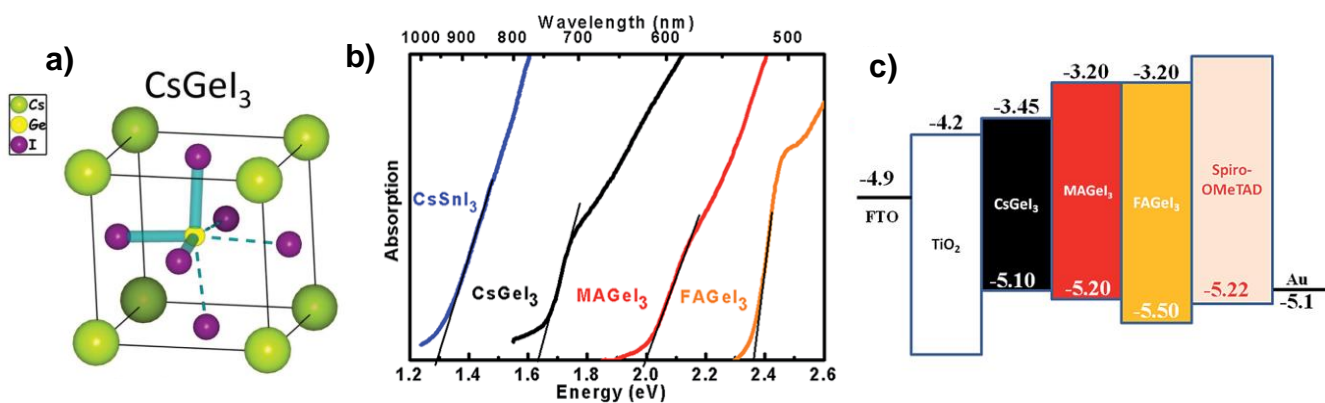


Figure 4. (a) Optimized geometrical crystal structure through image of the rhombohedrally distorted polar CsGeI₃ perovskite. Reproduced with permission.^[58] Copyright 2015, American Chemical Society. (b) Optical absorption spectrum of CsGeI₃, MAGeI₃ and FAGEI₃, in comparison with CsSnI₃ and (c) schematic energy level diagram of CsGeI₃, MAGeI₃ and FAGEI₃. Reproduced with permission.^[2] Copyright 2015 American Chemical Society.

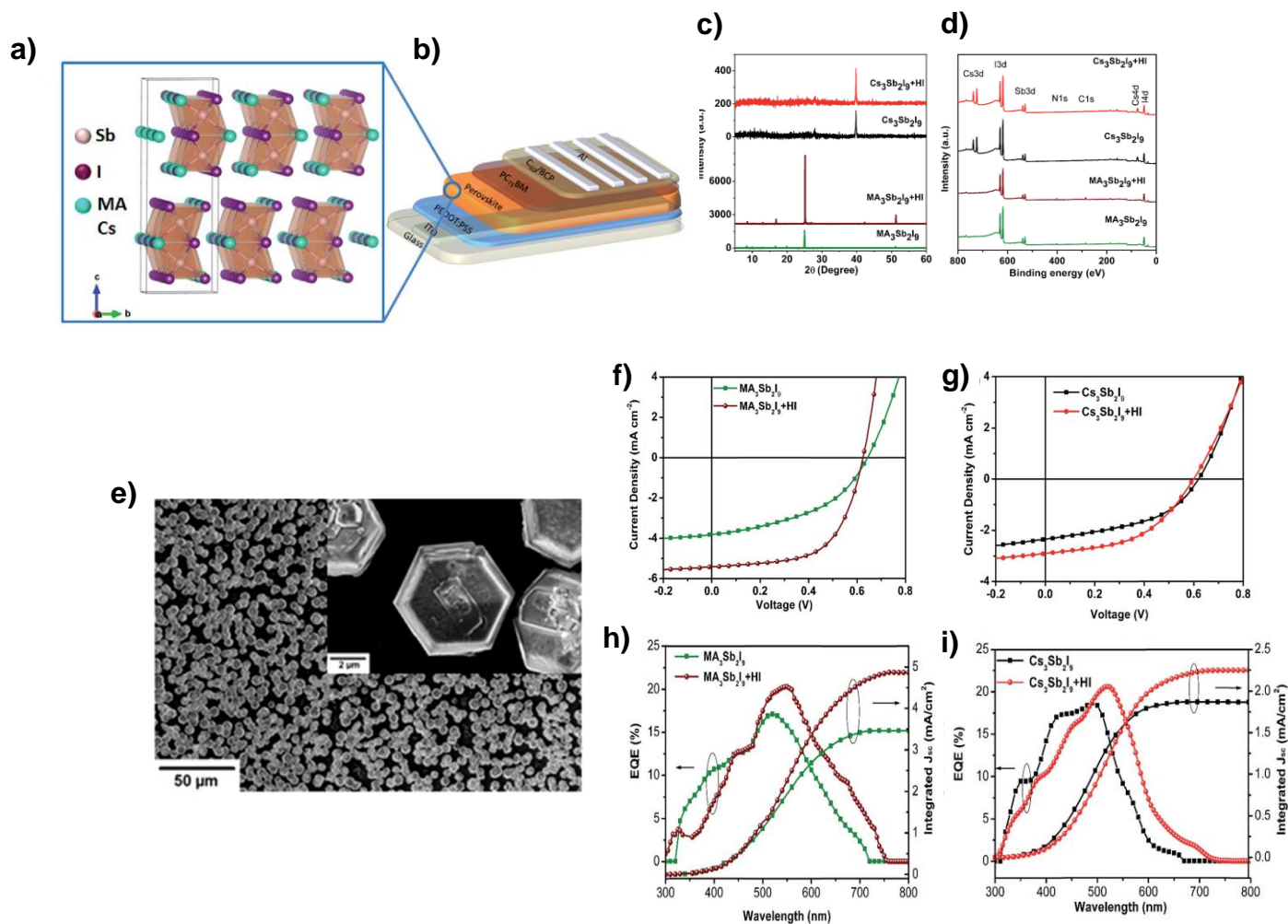


Figure 5. (a) Crystal structures of $A_3Sb_2I_9$ ($A = MA, Cs$) perovskite materials. (b) Schematic representation of a planar photovoltaic device structure incorporating Sb-based perovskite materials. (c) X-ray diffraction patterns and (d) X-ray photoelectron spectroscopy survey spectra of Sb-based perovskite films prepared with various cations. Reproduced with permission.^[110] Copyright 2017 American Chemical Society. (e) SEM image of the $(CH_3NH_3)_3Sb_2I_9$ thin film, showing hexagonal crystals after one-step spin coating. Reproduced with permission.^[98] Copyright 2016 American Chemical Society, J–V characteristics of (g) $MA_3Sb_2I_9$ and (h) $Cs_3Sb_2I_9$; EQE spectra of (i) $MA_3Sb_2I_9$ and (j) $Cs_3Sb_2I_9$. Reproduced with permission.^[110] Copyright 2017 American Chemical Society.

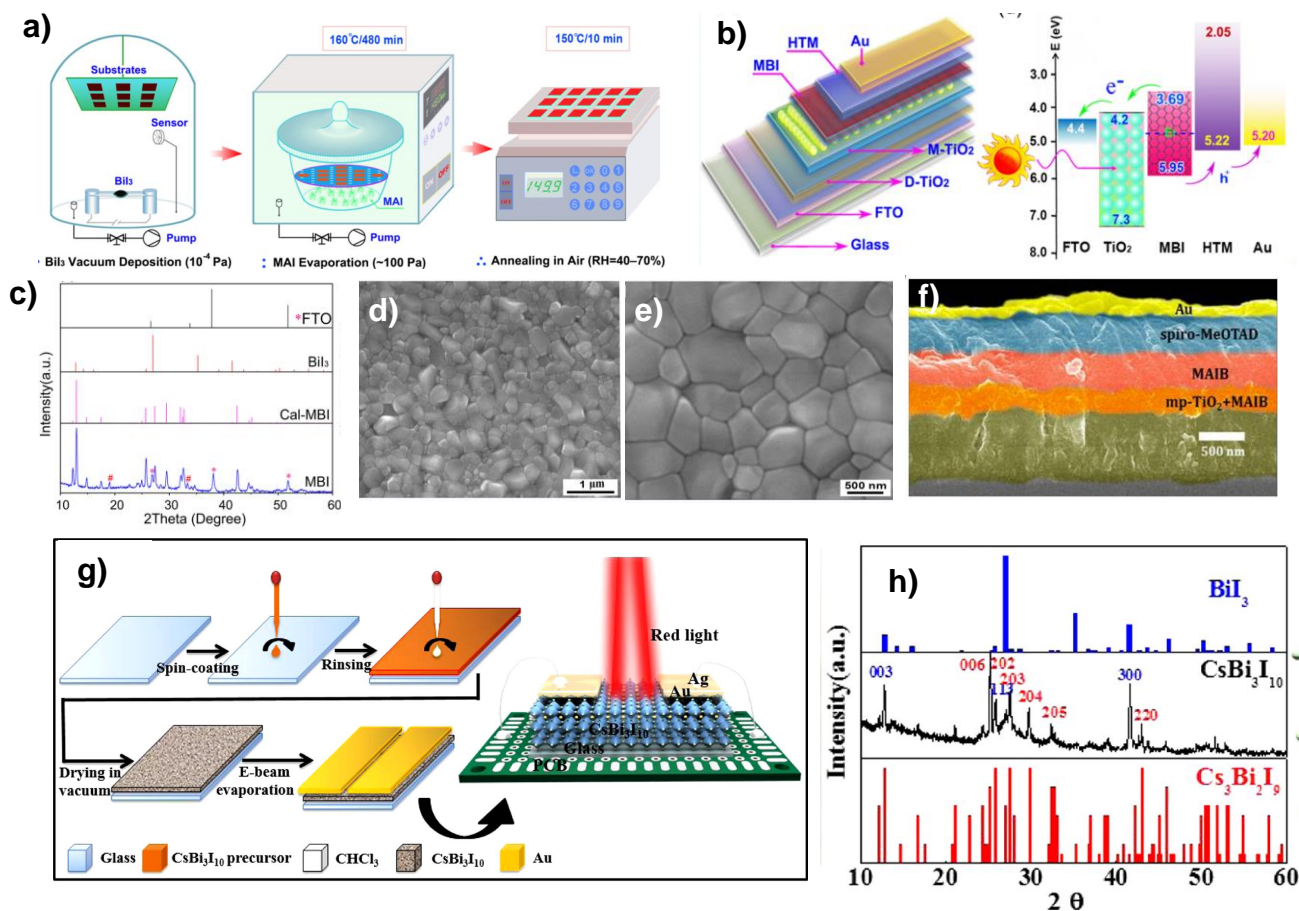


Figure 6. (a) Schematic illustration of the MBI film fabrication (b) structure of the target MBI solar cells (D-TiO₂: dense TiO₂; M-TiO₂: mesoporous TiO₂) as well as energy alignment of the components applied for the MBI solar cells. (c) XRD patterns for the MBI and BiI₃ films, FTO glass substrate, and the calculated MBI; The asterisked peaks in panel c are assigned to FTO, while the pound-marked peaks cannot be identified currently. SEM images for (d, e) 300 nm-thick MBI films (average RMS = 20.27 nm) by different magnification. Reproduced with permission.^[113] Copyright 2017 American Chemical Society. (f) Cross sectional image of fabricated MAIB device, Reproduced with permission.^[114] Copyright 2017 Wiley-VCH. (g) Schematic illustration of the stepwise process for the fabrication of the CsBi₃I₁₀ perovskite film photodetector. (h) XRD pattern of the CsBi₃I₁₀ perovskite film. Reproduced with permission.^[115] Copyright 2017 American Chemical Society.

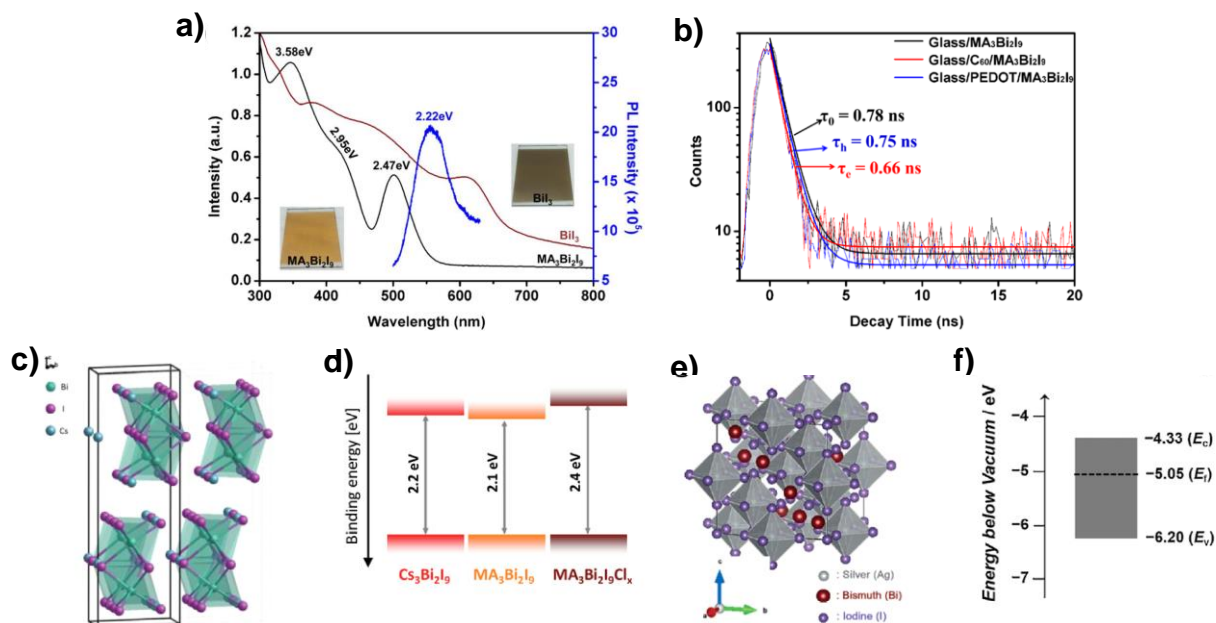


Figure 7. (a) UV-vis spectra of BiI_3 and $\text{MA}_3\text{Bi}_2\text{I}_9$ films and PL spectra of $\text{MA}_3\text{Bi}_2\text{I}_9$ film. Insets show photographs of the two films and (b) PL decay spectra of $\text{MA}_3\text{Bi}_2\text{I}_9$ film with different substrate. Reproduced with permission^[146] Copyright 2017, American Chemical Society. (c) Crystal structure of $\text{Cs}_3\text{Bi}_2\text{I}_9$, (d) band structure of different Bi-based PVKs, Reproduced with permission^[96] Copyright 2015, Wiley-VCH. (e) Crystal structure and (f) band structure of AgBi_2I_7 . Reproduced with permission.^[147] Copyright 2016, Wiley-VCH.

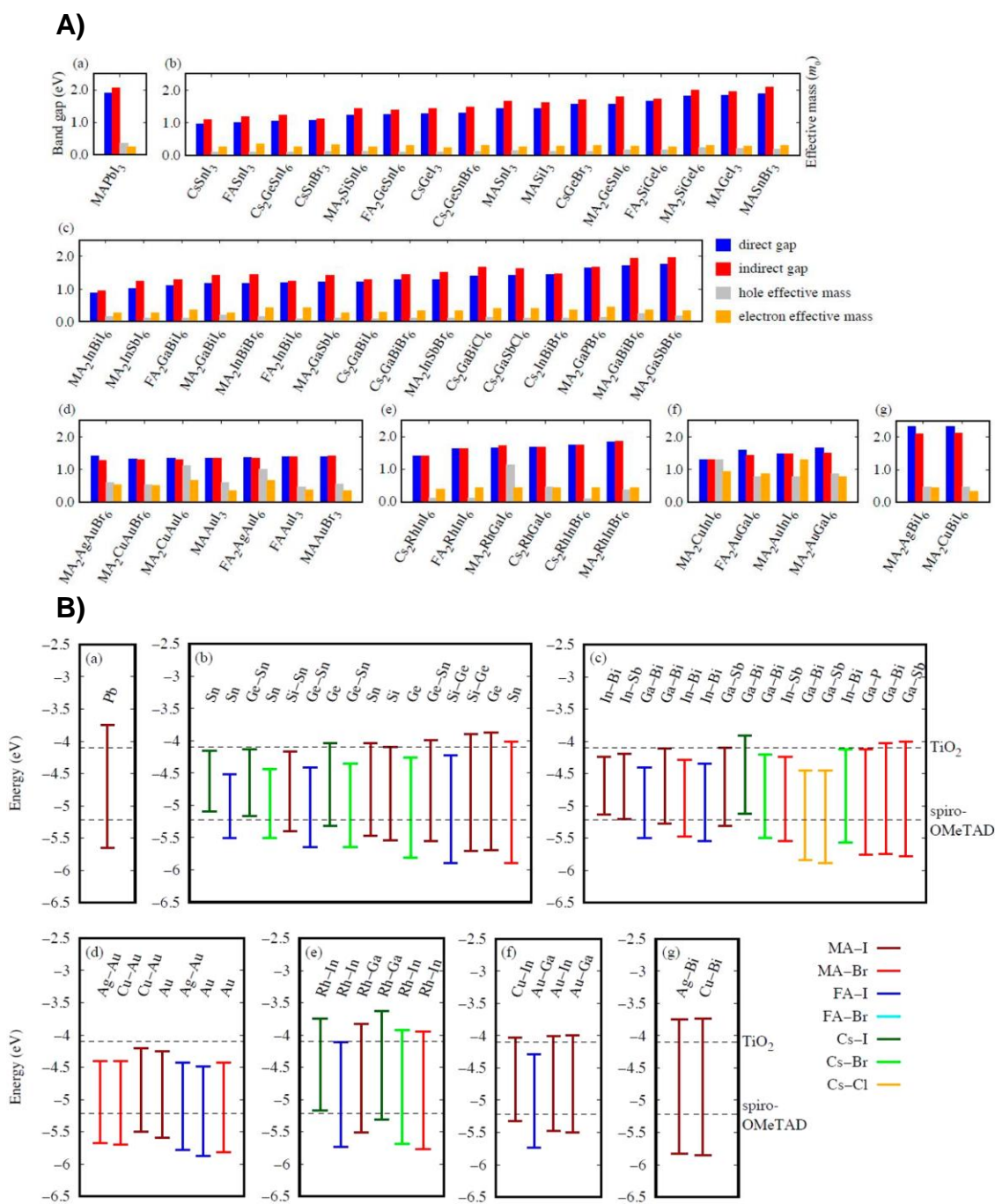


Figure 8. (A) Direct and indirect band gaps (in eV) and hole and electron absolute effective masses (in m_0) and (B) Positions of the band edges of VBM and CBM (in eV) for MAPbI₃ (a), group-14-group-14 (b), group-13-group-15 (c), group-11-group-11 (d), group-9-group-13 (e), group-11-group-13 (f), and group-11-group-15 (g) perovskites. Reproduced with permission.^[154] Copyright 2017 American Chemical Society.

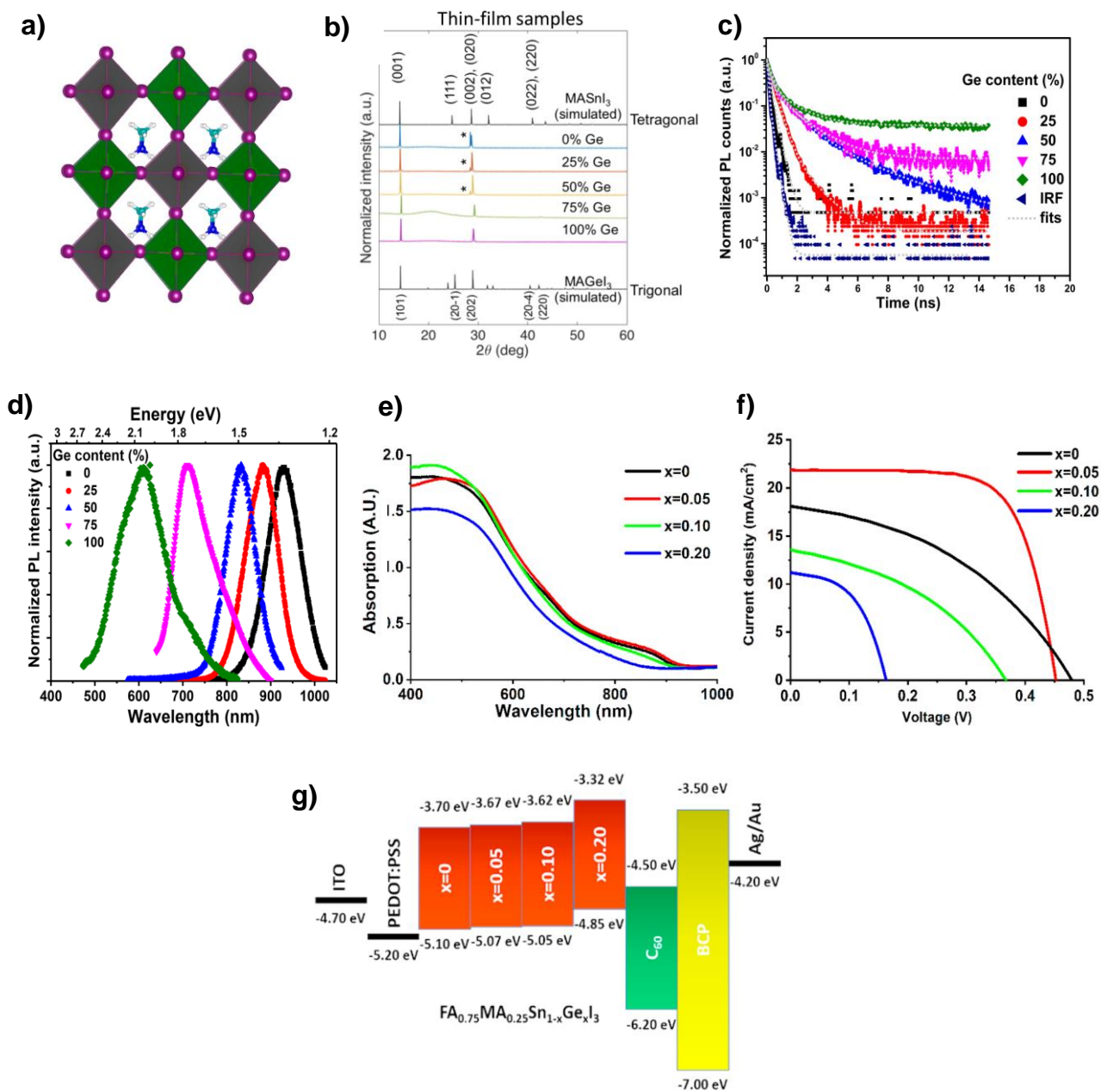


Figure 9. (a) Crystal structures of $\text{CH}_3\text{NH}_3\text{Sn}_{1-x}\text{Ge}_x\text{I}_3$ ($x = 0, 0.25, 0.50, 0.75, 1$) perovskite materials. (b) X-ray diffraction (XRD) patterns for 0% Ge ($\text{CH}_3\text{NH}_3\text{SnI}_3$), 25% Ge ($\text{CH}_3\text{NH}_3\text{Sn}_{0.75}\text{Ge}_{0.25}\text{I}_3$), 50% Ge ($\text{CH}_3\text{NH}_3\text{Sn}_{0.50}\text{Ge}_{0.50}\text{I}_3$), 75% Ge ($\text{CH}_3\text{NH}_3\text{Sn}_{0.25}\text{Ge}_{0.75}\text{I}_3$), and 100% Ge ($\text{CH}_3\text{NH}_3\text{GeI}_3$) thin films. * indicates small impurity phases. (c) PL decay of $\text{CH}_3\text{NH}_3\text{Sn}_{1-x}\text{Ge}_x\text{I}_3$. (d) Normalized photoluminescence (PL) spectra. Reproduced with permission.^[157] Copyright 2018 American Chemical Society. (e) UV-vis absorption. (f) J-V curve of the best performing devices for the $\text{FA}_{0.75}\text{MA}_{0.25}\text{Sn}_{1-x}\text{Ge}_x\text{I}_3$ materials. (g) Energy band diagram for every layer in the assembled solar cells. Reproduced with permission.^[158] Copyright 2018 American Chemical Society.

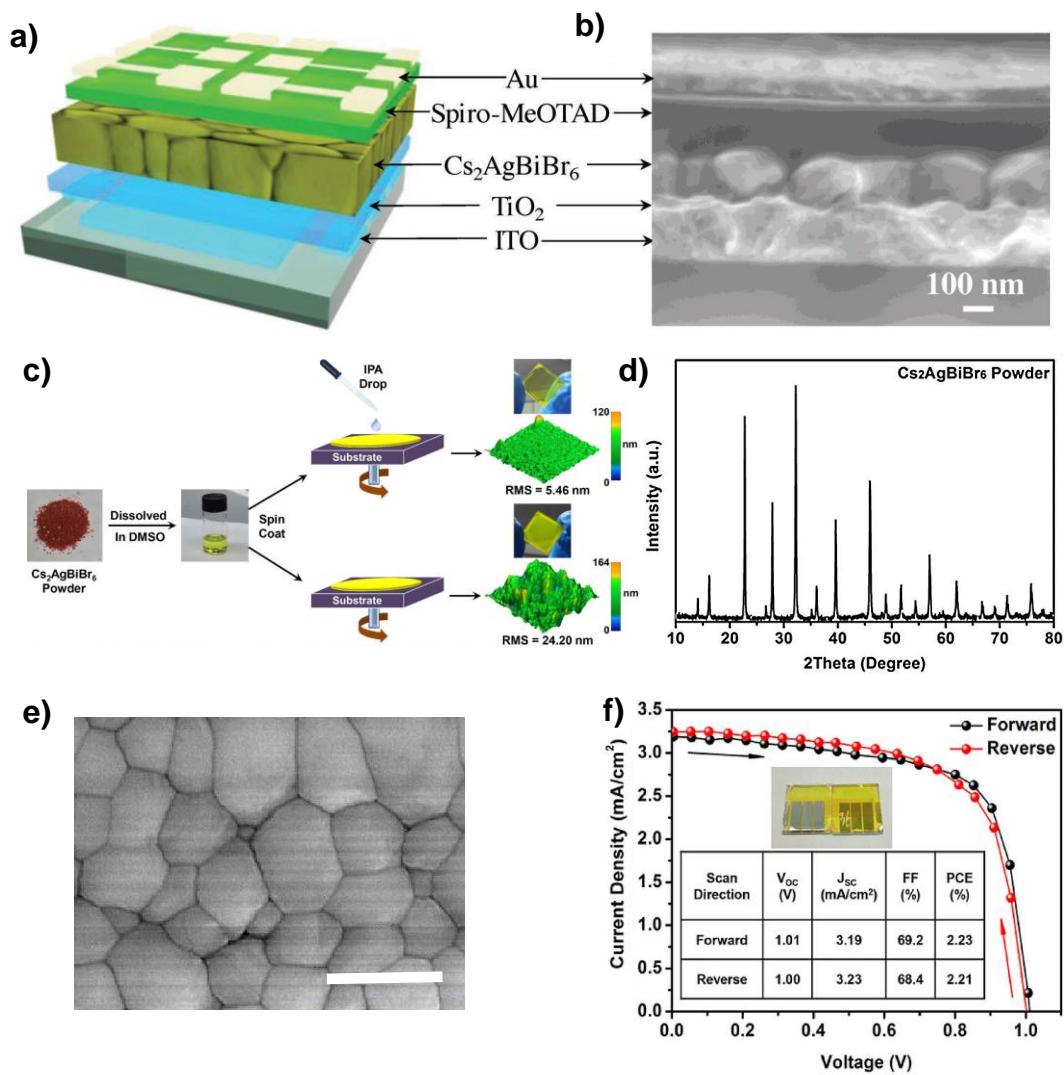


Figure 10. (a) $\text{Cs}_2\text{AgBiBr}_6$ solar cell structure, ITO/compact TiO_2 / $\text{Cs}_2\text{AgBiBr}_6$ /Spiro-OMeTAD/Au. (b) Cross-sectional SEM image of $\text{Cs}_2\text{AgBiBr}_6$ solar cells. Reproduced with permission.^[176] Copyright 2018 Wiley-VCH. (c) Schematic illustration of the spin-coating process (with and without anti-solvent dropping protocol) employed in this work. The morphology of the as-prepared film can be improved after IPA dropping. (d) XRD, (e) FESEM of the $\text{Cs}_2\text{AgBiBr}_6$ powder films with scale bar of 100 nm. (f) J - V curves for the forward and reverse scan directions for the best-performing PSCs. Reproduced with permission.^[175] Copyright 2018 Wiley-VCH.

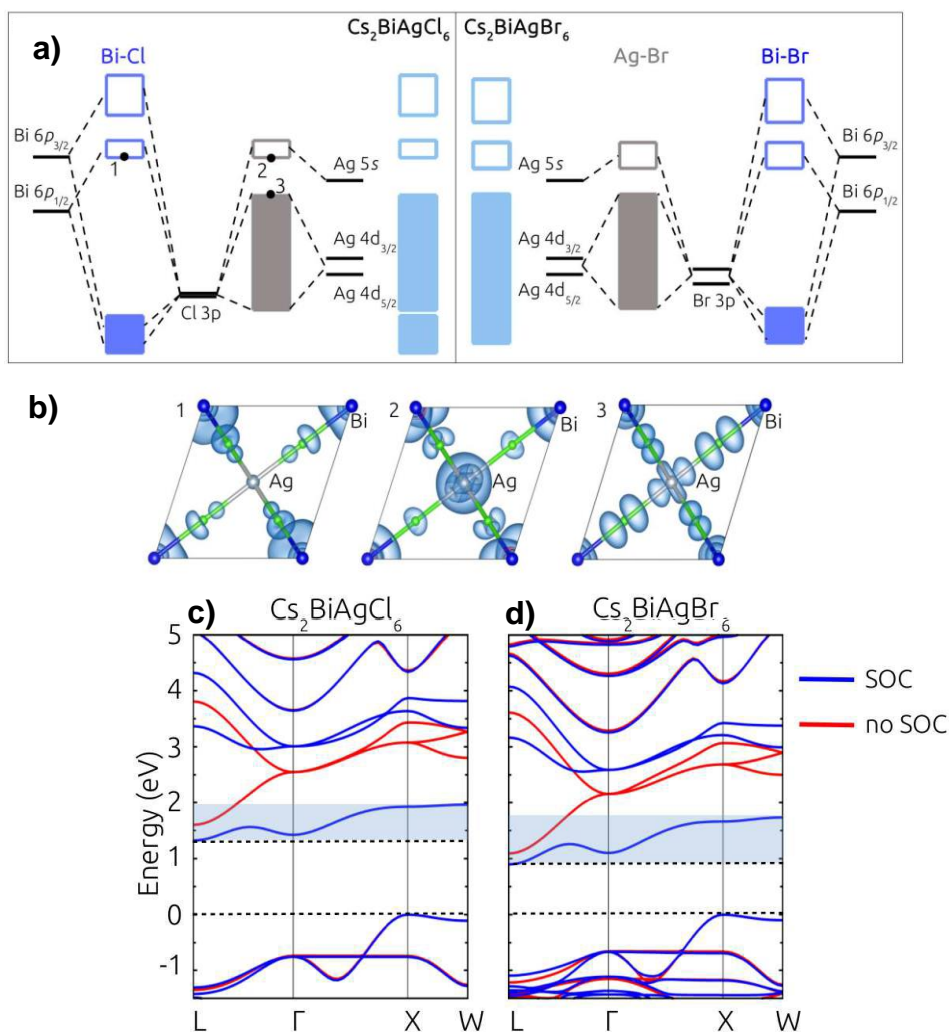


Figure 11. (a) Comparison of the molecular orbital diagrams Cs₂BiAgCl₆ (left) and Cs₂BiAgBr₆ (right). Black thick lines mark the atomic one-electron energies, dark blue rectangles correspond to the Bi-halide hybrid bands and the grey rectangles correspond to the Ag-halide hybrid bands. The light blue rectangles represent the bands formed in Cs₂BiAgCl₆ and Cs₂BiAgBr₆ respectively. Filled rectangles represent occupied (valence) bands, while the empty rectangles represent the unoccupied (conduction) bands. All bands are aligned with respect to the all-electron energy level of the Bi-5d_{1/2} and then red-shifted by 1.5 eV for visualization purposes. (b) Square modulus of the wave functions for states marked from 1 to 3 on the molecular orbital diagram of Cs₂BiAgCl₆. 1 represents the Bi-6p_{1/2}/halide-p antibonding orbitals at the bottom of the conduction band. 2 is the antibonding Ag-5s/halide-p at the L-point of the conduction band, while 3 corresponds to the Ag-4d/halide-p antibonding orbitals found at the top of the valence band. DFT-LDA band structure of Cs₂BiAgCl₆ (c) and Cs₂BiAgBr₆ (d). The calculations are performed with (blue lines) and without (red lines) spin-orbit coupling. The light blue shading highlights the width of the lowest conduction band as calculated from DFT+SOC: 0.6 eV for Cs₂BiAgCl₆ and 0.9 eV for Cs₂BiAgBr₆. Reproduced with permission.^[180] Copyright 2016 American Chemical Society.

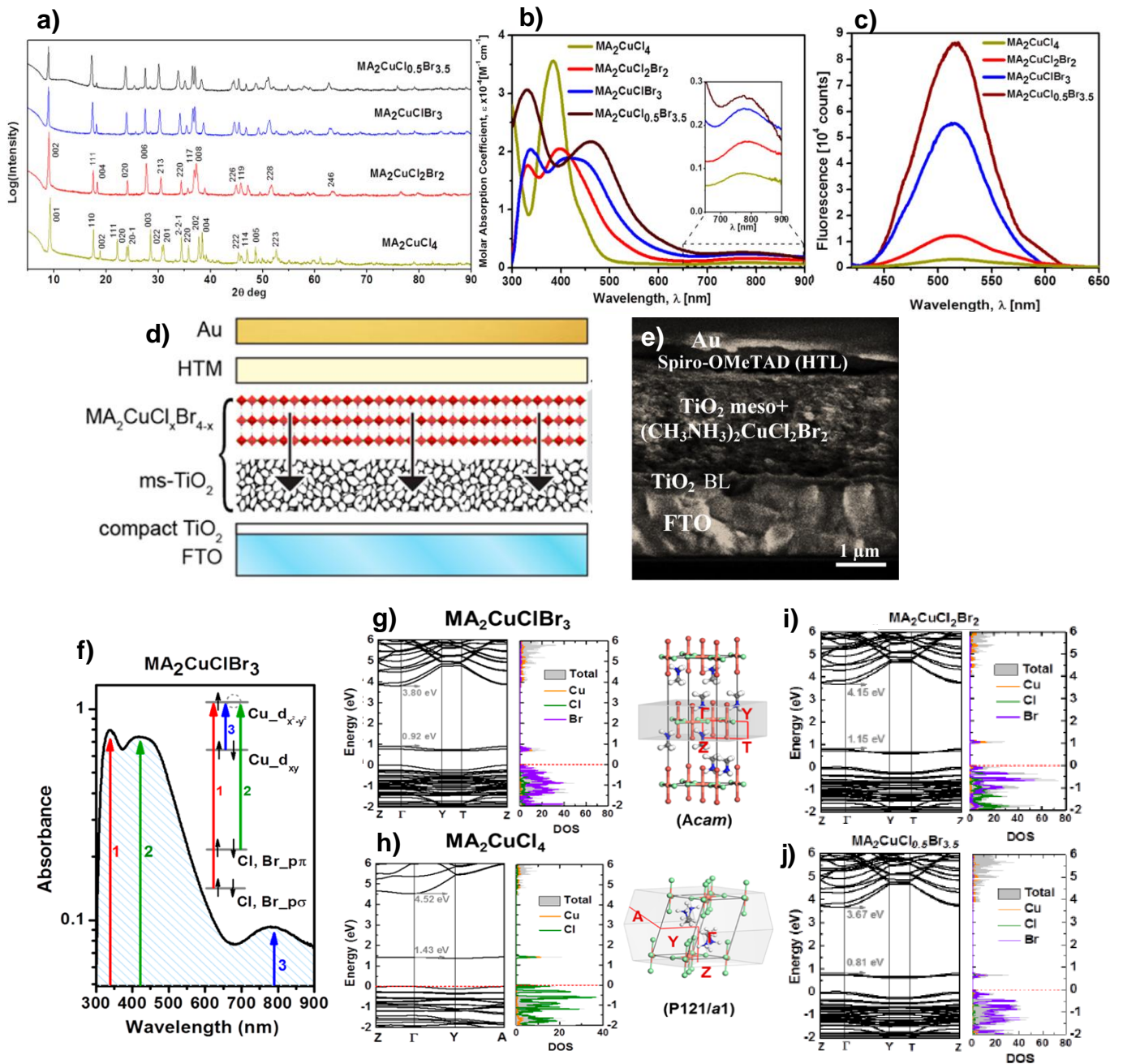


Figure 12. (a) XRD characterization of 2D copper-based perovskites: MA₂CuCl₄ (yellow), MA₂CuCl₂Br₂ (red), MA₂CuClBr₃ (blue), and MA₂CuCl_{0.5}Br_{3.5} (black); (b) Absorption coefficient for perovskites of the series MA₂CuCl_xBr_{4-x} showing strong CT bands below 650 nm and broad d-d transitions between 700 and 900 nm (inset). (c) Photoluminescence of the perovskites MA₂CuCl_xBr_{4-x} (λ_{exc} = 310 nm) with intensity increasing with higher Br contents. (d) Exploded view of solar cell devices based on mesoporous TiO₂ sensitized with the perovskite MA₂CuCl_xBr_{4-x}; Reproduced with permission.^[187] Copyright 2016 American Chemical Society. (e) Cross sectional SEM images of the solar cells with the configuration of glass/FTO/TiO₂/(CH₃NH₃)₂CuX (X = Cl₄, Cl₂, I₂, and Cl₂Br₂ materials) perovskite/spiro-OMeTAD (HTL)/Au. Reproduced with permission.^[13] Copyright 2018 American Chemical Society. (f) Representation of the electronic transitions for MA₂CuClBr₃: charge-transfer transitions 1 and 2 (Cl, Br_pσ → Cu_d_{x²-y²} and Cl, Br_pπ → Cu_d_{x²-y²}) and d-d transition 3 (Cu_d_{xy} → Cu_d_{x²-y²}); electronic band structure, density of states, and unit cell structure of the perovskite compounds (g) MA₂CuCl₄, (h) MA₂CuClBr₃, (i) MA₂CuCl₂Br₂ and (j) MA₂CuCl_{0.5}Br_{3.5} investigated by DFT simulation.^[187]

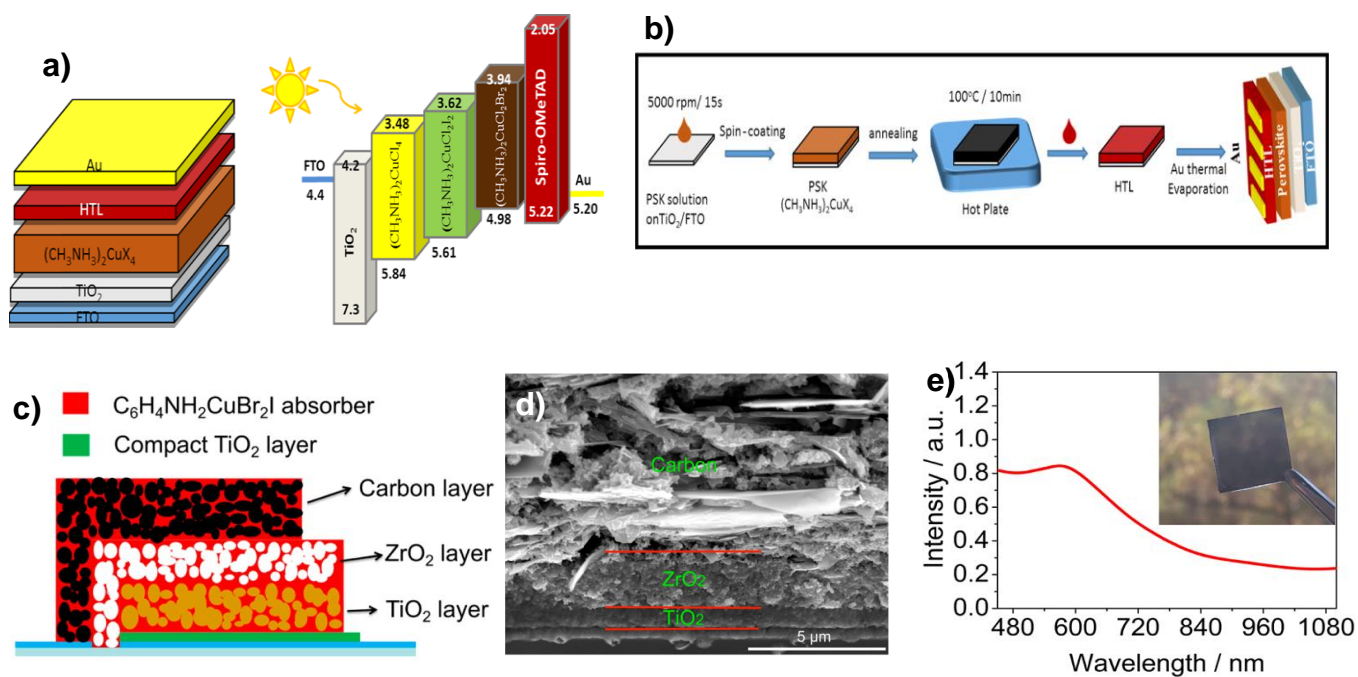


Figure 13. (a and b) Schematic diagram of the energy level diagram as well as the preparation of lead-free PSC step-by-step. Reproduced with permission.^[13] Copyright 2018 American Chemical Society. (c) Scheme and (d) cross section SEM image of the Cu-based solar cell. (e) UV/vis spectroscopy of $\text{C}_6\text{H}_4\text{NH}_2\text{CuBr}_2\text{I}$ thin film. Inset in panel b shows a picture of the thin film. Reproduced with permission.^[190] Copyright 2017 American Chemical Society.

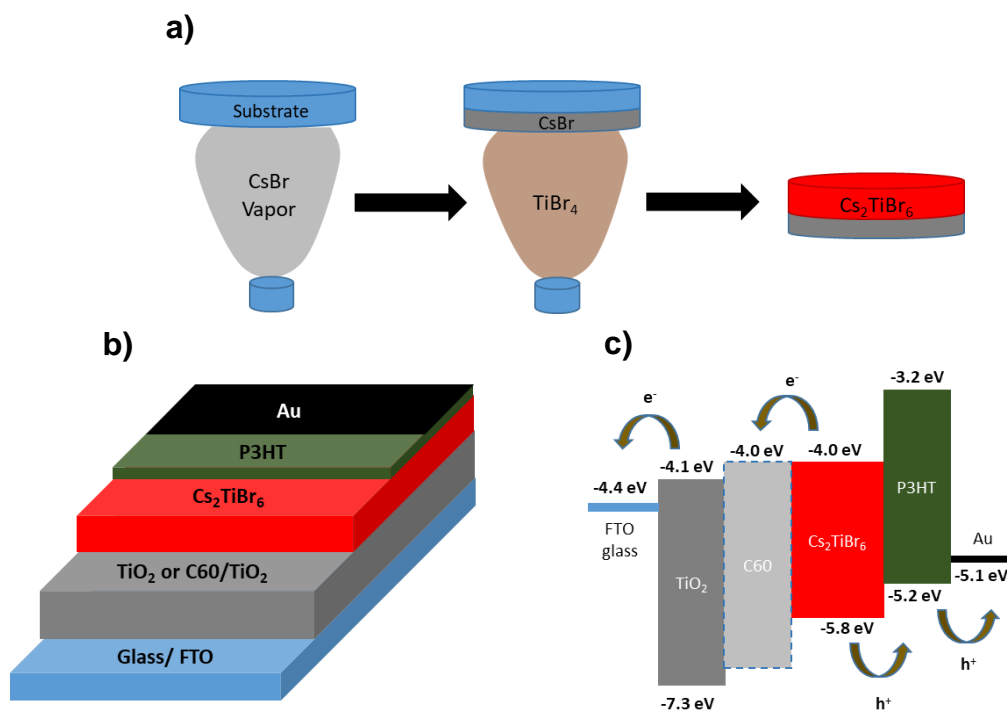


Figure 14. (a) Schematic illustration of the vapour-based synthesis of Cs_2TiBr_6 thin film. (b) Schematic illustrations and (c) energy levels of PSC architecture using the Cs_2TiBr_6 thin film as the light absorber in the PSC.

Table 1. Optical data and PV parameters of metal halide perovskites (ABX₃) along with the respective device structures: Homovalent substitution of the B site (Pb²⁺) with divalent tin (Sn²⁺) or germanium (Ge²⁺) cation

Absorber PSK ^a	Device structure ^a	E_g (eV)	PCE(%)	J_{sc} (mA/cm ²)	V_{oc} (V)	FF	Ref.
MASnI ₃	FTO/bl-TiO ₂ /mp-TiO ₂ /PSK/Spiro-OMeTAD/Au	1.23	6.40	16.80	0.88	0.42	[59]
MASnI ₃	FTO/bl-TiO ₂ /mp-TiO ₂ /PSK/Spiro-OMeTAD/Au	1.30	5.44	15.18	0.72	0.50	[60]
MASnI ₃	FTO/bl-TiO ₂ /mp-TiO ₂ /PSK/PTTA/Au	1.30	3.89	19.90	0.38	0.52	[61]
MASnI ₃	FTO/bl-TiO ₂ /mp-TiO ₂ /PSK/Au	1.30	3.15	21.40	0.32	0.46	[62]
MASnI ₃	ITO/PEDOT:PSS/PSK/C ₆₀ /BCP/Au	-	2.14	11.80	0.45	0.40	[63]
MASnI ₃	FTO/bl-TiO ₂ /mp-TiO ₂ /PSK/PTTA/Au	1.26	1.86	17.40	0.27	0.39	[64]
MASnI ₃	ITO/PEDOT:PSS/Poly-TPD/PSK/C ₆₀ /BCP/Au	1.30	1.70	12.10	0.38	0.37	[65]
MASnIBr ₂	FTO/bl-TiO ₂ /mp-TiO ₂ /PSK/Spiro-OMeTAD/Au	1.75	5.73	12.30	0.82	0.57	[51]
(MA) _{0.9} Cs _{0.1} SnI ₃	ITO/PEDOT:PSS/PSK/PCBM/Bis-C ₆₀ /Ag	1.41	0.3	4.50	0.20	0.36	[66]
(MA) _{0.9} Cs _{0.1} SnI ₃	FTO/bl-TiO ₂ /mp-TiO ₂ /PSK/PTTA/Au	2.13	0.51	2.24	0.49	0.46	[67]
(MA) _{0.9} Cs _{0.1} SnI ₃	FTO/bl-TiO ₂ /mp-TiO ₂ /PSK/P3HT/Au	2.20	1.12	4.27	0.50	0.49	[68]
MASnBr ₃ (CE)	FTO/bl-TiO ₂ /PSK/P3HT/Au	2.20	0.35	2.05	0.41	0.41	[68]
MASnBr ₃	FTO/bl-TiO ₂ /PSK/P3HT/Au	2.30	1.12	4.27	0.49	0.49	[68]
MASnI ₃	FTO/bl-TiO ₂ /mp-TiO ₂ /PSK/Spiro-OMeTAD/Au	1.30	3.89	19.92	0.37	0.51	[69]
MASnBr ₃	FTO/bl-TiO ₂ /mp-TiO ₂ /PSK/PTAA/Au	1.30	0.5	2.20	0.49	0.46	[67]
MASnBr ₃	FTO/bl-TiO ₂ /mp-TiO ₂ /PSK/P3HT/Au	1.30	1.1	4.30	0.50	0.49	[68]
FASnI ₃	FTO/bl-TiO ₂ /mp-TiO ₂ /PSK/Spiro-OMeTAD/Au	1.40	4.80	23.70	0.32	0.63	[70]
FASnI ₃	ITO/PEDOT:PSS/PSK/C ₆₀ /BCP/Ag	1.40	6.22	22.07	0.46	0.60	[71]
FASnI ₃	ITO/PEDOT:PSS/PSK/C ₆₀ /BCP/Ag	1.40	3.98	17.78	0.33	0.67	[72]
FASnI ₃	FTO/bl-TiO ₂ /mp-TiO ₂ /PSK/Spiro-OMeTAD/Au	1.63	5.50	19.80	0.41	0.66	[73]
FASnI ₃	ITO/PEDOT:PSS/PSK/C ₆₀ /BCP/Ag	1.36	6.60	21.30	0.48	0.64	[74]
FASnI ₃	FTO/bl-TiO ₂ /mp-TiO ₂ /ZnS/PSK/PTAA/Au	1.40	5.27	23.10	0.38	0.60	[75]
FASnI ₃	FTO/bl-TiO ₂ /mp-TiO ₂ /PSK/Spiro-OMeTAD/Au	1.41	2.10	24.50	0.24	0.36	[76]
(FA) _{0.75} (MA) _{0.25} SnI ₃	ITO/PEDOT:PSS/PSK/C ₆₀ /BCP/Ag	1.28	4.49	20.70	0.48	0.54	[74]
(FA) _{0.75} (MA) _{0.25} SnI ₃	ITO/PEDOT:PSS/PSK/C ₆₀ /BCP/Ag	1.30	5.92	21.30	0.53	0.52	[74]
(FA) _{0.75} (MA) _{0.25} SnI ₃	ITO/PEDOT:PSS/PSK/C ₆₀ /BCP/Ag	1.33	8.12	21.20	0.61	0.62	[74]
FA _{0.8} Cs _{0.2} SnI ₃	ITO/PEDOT:PSS/PSK/PCBM/Bis-C ₆₀ /Ag	1.33	1.40	16.10	0.24	0.36	[66]
FASnI ₃	ITO/PEDOT:PSS/PSK/C ₆₀ /BCP/Al	1.40	9.00	24.10	0.52	0.71	[77]
{en}FASnI ₃	FTO/bl-TiO ₂ /mp-TiO ₂ /PSK/PTTA/Au	1.50	7.14	22.50	0.48	0.66	[78]
(BA) ₂ (MA) ₃ Sn ₄ I ₁₃	FTO/bl-TiO ₂ /mp-TiO ₂ /PSK/PTTA/Au	1.42	2.53	24.10	0.23	0.46	[79]
FASn ₂ Br	ITO/PEDOT:PSS/PSK/C ₆₀ /Ca/Al	1.68	1.70	6.82	0.47	0.54	[80]
(PEA) ₂ (FA) ₈ Sn ₉ I ₂₈	ITO/NiO _x /PSK/PCBM/Al	1.78	5.94	14.44	0.59	0.69	[81]
{en}MASnI ₃	FTO/bl-TiO ₂ /mp-TiO ₂ /PSK/PTAA/Au	1.40	6.63	24.28	0.42	0.63	[82]
CsSnI ₃	FTO/bl-TiO ₂ /mp-TiO ₂ /PSK/m-MTDATA/Au	1.30	2.02	22.70	0.24	0.37	[52]

CsSnI ₃	FTO/bl-TiO ₂ /mp-TiO ₂ /PSK/m-MTDATA/Au	1.30	3×10^{-4}	0.19	0.01	0.21	[52]
CsSnI ₃	FTO/bl-TiO ₂ /mp-TiO ₂ /PSK/PTTA/Au	1.30	4.81	25.71	0.38	0.49	[83]
CsSnI ₃	ITO/PSK/PC61BM/BCP/Al	1.30	3.56	9.89	0.50	0.68	[84]
CsSnI ₃	ITO/NiO _x /PSK/PCBM/Al	1.30	3.31	10.2	0.52	0.62	[85]
CsSnI ₃	ITO/CuI/PSK/ICBA/BCP/Al	1.30	2.76	12.3	0.43	0.39	[85]
CsSnI ₃	FTO/bl-TiO ₂ /mp-TiO ₂ /PSK/PTTA/Au	1.25	1.83	30.8	0.17	0.34	[61]
CsSnI ₃	FTO/bl-TiO ₂ /mp-TiO ₂ /PSK/Au	1.27	1.66	27.7	0.20	0.29	[86]
CsSnI ₃	ITO/PSK/C ₆₀ /Au/Ti	1.30	0.88	4.8	0.42	0.22	[87]
CsSnI ₃ :CsSnBr ₃ (1:1)	FTO/bl-TiO ₂ /mp-TiO ₂ /PSK/m-MTDATA/Au	1.50	0.13	3.69	0.14	0.26	[86]
CsSnI ₂ Br	FTO/bl-TiO ₂ /mp-TiO ₂ /PSK/Spiro-OMeTAD/Au	1.37	1.67	15.06	0.28	0.38	[86]
CsSnI ₂ Br	FTO/bl-TiO ₂ /mp-TiO ₂ /PSK/Spiro-OMeTAD/Au	1.37	3.20	16.70	0.33	0.53	[88]
CsSnBr ₃	FTO/bl-TiO ₂ /mp-TiO ₂ /PSK/Spiro-OMeTAD/Au	1.75	2.17	9.10	0.42	0.57	[89]
CsSnI ₂ Br ₂ (HPA)	FTO/bl-TiO ₂ /mp-TiO ₂ /Al ₂ O ₃ /PV/C	1.63	3.00	16.70	0.33	0.53	[88]
CsSnI ₃	ITO/NiO _x /PSK/PCBM/Al	1.30	3.31	10.21	0.52	0.62	[84]
CsSnI ₃ (SnCl ₂)	ITO/PSK/PCBM/BCP/Al	1.30	3.56	10.44	0.51	0.69	[90]
CsSnI ₃	FTO/bl-TiO ₂ /mp-TiO ₂ /PSK/PTAA/Au	1.30	4.81	25.71	0.38	0.49	[91]
Cs ₂ SnI ₆	FTO/bl-ZnO/nanorods/PSK/P3HT/Ag	1.48	0.86	3.20	0.52	0.51	[92]
Cs ₂ SnI ₆ (from CsSnI ₃)	FTO/bl-TiO ₂ /PSK/P3HT/Ag	1.48	0.96	5.41	0.51	0.35	[93]
Cs ₂ SnI ₄ Br ₂	FTO/bl-TiO ₂ /mp-2 wt% Sn-TiO ₂ /PSK/solid state Cs ₂ SnI ₆ based HTM/LPAH/FTO	1.40	2.02	6.22	0.56	0.57	[94]
MA _{0.9} Cs _{0.1} SnI ₃	ITO/NiO _x /PSK/PCBM/Al	-	0.30	4.50	0.20	0.36	[72]
CsGeI ₃	FTO/bl-TiO ₂ /mp-TiO ₂ /PSK/Spiro-OMeTAD/Au	1.63	0.01	5.70	0.07	0.27	[9]
MAGeI ₃	FTO/bl-TiO ₂ /mp-TiO ₂ /PSK/Spiro-OMeTAD/Au	2.00	0.20	4.00	0.15	0.30	[9]

Table 2. Optical data and PV parameters of metal halide perovskites (ABX₃) along with the respective device structures: heterovalent substitution of the B site (Pb²⁺) with trivalent Sb³⁺ and Bi³⁺ cation

Absorber ^a	Device structure ^a	E _g (eV)	PCE(%)	J _{sc} (mA/cm ²)	V _{oc} (V)	FF	Ref.
MA ₃ Sb ₂ I ₉	ITO/PEDOT:PSS/PSK/PCBM/C ₆₀ /BCP/Al	1.95	2.04	5.41	0.62	0.60	[116]
MA ₃ Sb ₂ I ₉	ITO/PEDOT:PSS/PSK/PC ₆₁ BM/ZnO-NP/Al	2.14	0.49	1.00	0.90	0.55	[98]
Rb ₃ Sb ₂ I ₉	FTO/bl-TiO ₂ /mp-TiO ₂ /PSK/Poly-TPD/Au	2.24	0.66	2.11	0.55	0.56	[117]
(NH ₄) ₃ Sb ₂ I ₉	ITO/PEDOT:PSS/PSK/PC ₆₁ BM/Al	2.27	0.51	1.15	1.03	0.42	[118]
Cs ₃ Sb ₂ I ₉	FTO/bl-TiO ₂ /PSK/PTAA/Au	2.05	<1.00	- (e)	0.25e0.30	- (e)	[99]
Cs ₃ Sb ₂ I ₉	ITO/PEDOT:PSS/PSK/PCBM/BCP/Al	2.05	1.49	5.31	0.72	0.38	[119]
Cs ₃ Sb ₂ I ₉	ITO/PEDOT:PSS/PSK/PC ₆₁ BM/C ₆₀ /BCP/Al	2.05	0.84	2.91	0.60	0.48	[116]
MA ₃ Sb ₂ Cl _x I _{9-x}	FTO/bl-TiO ₂ /mp-TiO ₂ /PSK/Spiro-OMeTAD/Au	1.79	2.19	5.04	0.69	0.63	[120]
Cs ₃ Bi ₂ I ₉	FTO/bl-TiO ₂ /mp-TiO ₂ /PSK/Spiro-OMeTAD/Ag	2.20	1.09	2.15	0.85	0.60	[96]
Cs ₃ Bi ₂ I ₉	FTO/bl-TiO ₂ /mp-TiO ₂ /PSK/P3HT/Ag	2.20	0.02	0.18	0.26	0.37	[121]
CsBi ₃ I ₁₀	FTO/bl-TiO ₂ /mp-TiO ₂ /PSK/P3HT/Ag	1.77	0.40	3.40	0.31	0.38	[121]
MA ₃ Bi ₂ I ₉	FTO/bl-TiO ₂ /mp-TiO ₂ /PSK/Spiro-OMeTAD/Ag	2.10	0.12	0.52	0.68	0.33	[96]
MA ₃ Bi ₂ I ₉	FTO/bl-TiO ₂ /mp-TiO ₂ /PSK/P3HT/Au	2.10	0.19	1.16	0.35	0.46	[122]
MA ₃ Bi ₂ I ₉	FTO/bl-TiO ₂ /mp-TiO ₂ /PSK/Spiro-OMeTAD/Ag	2.10	0.08	0.36	0.51	0.44	[122]
MA ₃ Bi ₂ I ₉	FTO/bl-TiO ₂ /mp-TiO ₂ /PSK/Spiro-OMeTAD/Au	2.10	0.26	0.83	0.56	0.48	[123]
MA ₃ Bi ₂ I ₉	FTO/bl-TiO ₂ /mp-TiO ₂ /PSK/Spiro-OMeTAD/Ag	2.10	0.09	0.57	0.53	0.30	[123]
MA ₃ Bi ₂ I ₉	FTO/bl-TiO ₂ /mp-TiO ₂ /PSK/Spiro-OMeTAD/Ag	2.10	0.11	0.61	0.51	0.33	[123]
MA ₃ Bi ₂ I ₉	FTO/bl-TiO ₂ /mp-TiO ₂ /PSK/Spiro-OMeTAD/MoO ₃ /Ag	2.10	0.42	1.00	0.67	0.62	[124]
MA ₃ Bi ₂ I ₉	FTO/bl-TiO ₂ /mp-TiO ₂ /PSK/Spiro-OMeTAD/Ag	2.10	0.14	0.49	0.67	0.35	[124]
MA ₃ Bi ₂ I ₉	FTO/bl-TiO ₂ /mp-TiO ₂ /PSK/Spiro-OMeTAD/Ag	2.10	0.02	0.13	0.45	0.36	[125]
MA ₃ Bi ₂ I ₉	FTO/bl-TiO ₂ /mp-TiO ₂ /PSK/Spiro-OMeTAD/Ag	2.10	0.05	0.17	0.84	0.35	[125]
MA ₃ Bi ₂ I ₉	ITO/PEDOT:PSS/PSK/C ₆₀ /BCP/Ag	2.10	0.39	1.39	0.83	0.34	[126]
MA ₃ Bi ₂ I ₉	FTO/bl-TiO ₂ /mp-TiO ₂ /PSK/Spiro-OMeTAD/Au	2.10	0.36	1.10	0.65	0.50	[127]
MA ₃ Bi ₂ I ₉	FTO/bl-TiO ₂ /mp-TiO ₂ /PSK/Spiro-OMeTAD/Au	2.10	0.31	0.94	0.51	0.61	[128]
MA ₃ Bi ₂ I ₉	FTO/bl-TiO ₂ /mp-TiO ₂ /PSK/Spiro-OMeTAD/Au	2.10	0.11	0.49	0.72	0.32	[129]
MA ₃ Bi ₂ I ₉	FTO/bl-TiO ₂ /mp-TiO ₂ /PSK/Spiro-OMeTAD/Au	2.10	0.25	0.83	0.56	0.56	[123]
MA ₃ Bi ₂ I ₉	FTO/bl-TiO ₂ /mp-TiO ₂ /PSK/Spiro-OMeTAD/Au	2.10	1.64	2.95	0.81	0.69	[130]
MA ₃ Bi ₂ I ₉	ITO/PEDOT:PSS/PV/PCBM/Ca/Au	2.90	0.07	0.22	0.66	0.49	[136]
MA ₃ Bi ₂ I ₉ Cl _x	FTO/bl-TiO ₂ /mp-TiO ₂ /PSK/Spiro-OMeTAD/Ag	2.40	0.003	0.18	0.04	0.38	[96]
(MA ₃ Bi ₂ I ₉) _{0.2} (BiI ₃) _{0.8}	FTO/bl-TiO ₂ /mp-TiO ₂ /PV/PTAA/PIDT-DFBT/Ag	-	0.08	0.57	0.27	0.50	[131]
C ₅ H ₈ NBiI ₄	FTO/bl-TiO ₂ /mp-TiO ₂ /PSK/Spiro-OMeTAD/Au	1.98	0.90	2.71	0.62	0.54	[132]
(H ₃ NC ₆ H ₁₂ NH ₃)BiI ₅	FTO/bl-TiO ₂ /mp-TiO ₂ /PSK/Spiro-OMeTAD/Au	2.10	0.03	0.12	0.40	0.43	[122]

Table 3. Optical data and PV parameters of metal halide perovskites (ABX₃) based solar cells along with the respective device structures: heterovalent substitution of the B site (Pb²⁺) with double cation (Ag-Bi) and (Sn-Ge).

Absorber PSK ^a	Device structure ^a	E _g (eV)	PCE(%)	J _{sc} (mA/cm ²)	V _{oc} (V)	FF	Ref.
Ag ₃ BiI ₆	FTO/bl-TiO ₂ /mp-TiO ₂ /PSK/PTAA/Au	1.83	4.30	10.70	0.63	0.64	[181]
AgBi ₂ I ₇	FTO/bl-TiO ₂ /mp-TiO ₂ /PSK/P3HT/Ag	1.87	1.22	3.30	0.56	0.67	[182]
Ag ₂ BiI ₅	FTO/bl-TiO ₂ /mp-TiO ₂ /PSK/P3HT/Au	1.85	2.10	6.80	0.49	0.63	[183]
Cs ₂ AgBiBr ₆	ITO/PEDOT:PSS/PSK/PCBM/BCP/Al	2.05	1.44	1.78	1.04	0.78	[184]
Cs ₂ AgBiBr ₆	FTO/bl-TiO ₂ /mp-TiO ₂ /PSK/Spiro-OMeTAD/Au	2.21	2.43	3.93	0.98	0.63	[185]
FA _{0.75} MA _{0.25} Sn _{0.95} Ge _{0.05} I ₃	ITO/PEDOT:PSS/PSK/C ₆₀ /BCP/Au	1.40	4.48	19.50	0.42	0.55	[158]
FA _{0.75} MA _{0.25} Sn _{0.9} Ge _{0.1} I ₃	ITO/PEDOT:PSS/PSK/C ₆₀ /BCP/Au	1.42	2.04	13.27	0.33	0.49	[158]
FA _{0.75} MA _{0.25} Sn _{0.8} Ge _{0.2} I ₃	ITO/PEDOT:PSS/PSK/C ₆₀ /BCP/Au	1.53	0.08	11.84	0.15	0.46	[158]

Table 4. Optical data and PV parameters of lead free metal halide based perovskite solar cells: substitution of the B site with transition metal Cu or Ti

Absorber ^a	Device structure ^a	E _g (eV)	PCE(%)	J _{sc} (mA/cm ²)	V _{oc} (V)	FF	Ref.
MA ₂ CuCl ₂ Br ₂	FTO/bl-TiO ₂ /mp-TiO ₂ /PSK/Spiro-OMeTAD/Au	2.12	0.01	0.21	0.25	0.32	[187]
MA ₂ CuCl _{0.5} Br _{3.5}	FTO/bl-TiO ₂ /mp-TiO ₂ /PSK/Spiro-OMeTAD/Au	1.80	0.002	0.021	0.29	0.28	[187]
(p-F-C ₆ H ₅ C ₂ H ₄ NH ₃) ₂ CuBr ₄	FTO/bl-TiO ₂ /mp-TiO ₂ /PSK/Spiro-OMeTAD/Ag	1.74	0.51	1.46	0.87	0.40	[193]
(CH ₃ (CH ₂) ₃ NH ₃) ₂ CuBr ₄	FTO/bl-TiO ₂ /mp-TiO ₂ /PSK/Spiro-OMeTAD/Ag	1.76	0.63	1.78	0.88	0.40	[193]
C ₆ H ₄ NH ₂ CuBr ₂ I	FTO/bl-TiO ₂ /mp-TiO ₂ /PSK/ZrO ₂ /C	1.64	0.46	6.20	0.20	0.46	[190]
Cs ₂ TiBr ₆	FTO/bl-TiO ₂ /PSK/P3HT/Au	1.80	2.15	4.03	0.89	0.63	[191]
Cs ₂ TiBr ₆ with C ₆₀	FTO/C ₆₀ -TiO ₂ /PSK/P3HT/Au	1.80	3.22	5.69	1.02	0.56	[191]